NAVAL POSTGRADUATE SCHOOL
Monterey, California

THESIS

AN INVESTIGATION OF ACOUSTIC CAVITATION PRODUCED BY PULSED ULTRASOUND

by

Robert L. Bruce, Jr.
and
Robert D. Middleton, Jr.

December 1987

Thesis Advisor: Anthony A. Atchley

Approved for public release; distribution is unlimited.

SECURITY CLASSIFICATION OF THIS PAGE

REPORT DOCUMENTATION PAGE

1a REPORT SECURITY CLASSIFICATION UNCLASSIFIED	1b RESTRICTIVE MARKINGS
2a SECURITY CLASSIFICATION AUTHORITY	3 DISTRIBUTION / AVAILABILITY OF REPORT Approved for public release; distribution is unlimited.
2b DECLASSIFICATION / DOWNGRADING SCHEDULE	
4 PERFORMING ORGANIZATION REPORT NUMBER(S)	5 MONITORING ORGANIZATION REPORT NUMBER(S)
6a NAME OF PERFORMING ORGANIZATION Naval Postgraduate School 6b OFFICE SYMBOL (*If applicable*) 61	7a NAME OF MONITORING ORGANIZATION Naval Postgraduate School
6c. ADDRESS (*City, State, and ZIP Code*) Monterey, California 93943-5000	7b. ADDRESS (*City, State, and ZIP Code*) Monterey, California 93943-5000
8a NAME OF FUNDING / SPONSORING ORGANIZATION 8b OFFICE SYMBOL (*If applicable*)	9. PROCUREMENT INSTRUMENT IDENTIFICATION NUMBER
8c. ADDRESS (*City, State, and ZIP Code*)	10 SOURCE OF FUNDING NUMBERS PROGRAM ELEMENT NO. / PROJECT NO / TASK NO / WORK UNIT ACCESSION NO

11 TITLE (*Include Security Classification*)

AN INVESTIGATION OF ACOUSTIC CAVITATION PRODUCED BY PULSED ULTRASOUND

12 PERSONAL AUTHOR(S)

BRUCE, Robert L., and MIDDLETON, Robert D., Jr.

13a. TYPE OF REPORT	13b TIME COVERED	14. DATE OF REPORT (*Year, Month, Day*)	15 PAGE COUNT
Master's Thesis	FROM _____ TO _____	1987 December	95

16 SUPPLEMENTARY NOTATION

17 COSATI CODES			18 SUBJECT TERMS (*Continue on reverse if necessary and identify by block number*)
FIELD	GROUP	SUB-GROUP	Microcavitation, Cavitation Threshold, Threshold Detection, Transducer Calibration

19 ABSTRACT (*Continue on reverse if necessary and identify by block number*)

Transient cavitation produced by pulsed ultrasound in the MHz range has been investigated. First, a theoretical background which develops bubble motion in general and focuses specifically on transient cavitation is presented. Second, the development of an apparatus which is designed specifically for studying this type of cavitation is discussed. Third, the use of the apparatus to make measurements of cavitation thresholds at various frequencies, pulse durations, and pulse repetition rates is discussed. Finally, results of the cavitation threshold measurements are interpreted using theories developed earlier.

20 DISTRIBUTION / AVAILABILITY OF ABSTRACT ☒ UNCLASSIFIED/UNLIMITED ☐ SAME AS RPT ☐ DTIC USERS	21. ABSTRACT SECURITY CLASSIFICATION UNCLASSIFIED
22a NAME OF RESPONSIBLE INDIVIDUAL Professor A.A. Atchley, Code 61Ay	22b TELEPHONE (*Include Area Code*) 408-646-2848 22c. OFFICE SYMBOL 61Ay

DD FORM 1473, 84 MAR 83 APR edition may be used until exhausted. All other editions are obsolete

SECURITY CLASSIFICATION OF THIS PAGE

☆ U.S. Government Printing Office: 1986—606-24

Approved for public release; distribution is unlimited.

An Investigation of Acoustic Cavitation Produced by Pulsed Ultrasound

by

Robert L. Bruce, Jr.
Lieutenant Commander, United States Navy
B.A., University of Texas, 1975

and

Robert D. Middleton, Jr.
Lieutenant, United States Navy
B.S., Tulane University, 1980

Submitted in partial fulfillment of the
requirements for the degree of

MASTER OF SCIENCE IN ENGINEERING ACOUSTICS

from the

NAVAL POSTGRADUATE SCHOOL
December 1987

ABSTRACT

Transient cavitation produced by pulsed ultrasound in the MHz range has been investigated. First, a theoretical background which develops bubble motion in general and focuses specifically on transient cavitation is presented. Second, the development of an apparatus which is designed specifically for studying this type of cavitation is discussed. Third, the use of the apparatus to make measurements of cavitation thresholds at various frequencies, pulse durations, and pulse repetition rates is discussed. Finally, results of the cavitation threshold measurements are interpreted using theories developed earlier.

TABLE OF CONTENTS

ACKNOWLEDGMENTS

The following people helped us greatly by providing their knowledge, skills, forebearance, and/or personal dedication:

Anthony A. Atchley

George Jaksha

Steve Blankschein

Carol Crooker

Maria Zanger

Amy and Aaron Bruce

Our classmates in UX 61

I. INTRODUCTION

The term "cavitation" was first used in the late nineteenth century by Sir Charles Parsons to describe the mechanism that caused reduced thrust in marine propellers. Lord Rayleigh, in 1917, identified cavitation as the cause of erosion in pump components that were subject to reduced liquid pressures. Cavitation has come to be defined as the rupture of a liquid or a liquid/solid interface due to the reduction of liquid pressure [Ref. 1]. Since the theoretical tensile strength of pure liquids is exceptionally high, extremely large negative pressures ($\approx$ -1000 bars) should be required to cause the liquid bonds to break.

Since rupture in real liquids can occur at relatively low negative pressures ($\approx$ -1 bar), it has been postulated that inhomogeneities exist within the fluid which cause this reduced tensile strength. Furthermore, experimental results point to the necessity of these microscopic inhomogeneities containing gas [Ref. 2]. Thus, cavitation is actually the formation of macroscopic bubbles from microscopic bubbles (cavitation nuclei). Acoustic cavitation can therefore be defined as the activity of bubbles within a liquid that is subject to an acoustic pressure field.

Microcavitation, or the formation of micron-sized bubbles from cavitation nuclei due to the influence of ultrasonic acoustic energy (ultrasound), has benefits when used in such applications as ultrasonic cleaning and etching, acceleration of certain chemical reactions, and, medically, to destroy unwanted cell formations. Microcavitation may,

however, produce adverse biological effects as well. In particular, the improper use of diagnostic or therapeutic ultrasound could possibly result in the unintentional destruction of or damage to healthy cells.

Investigation of microcavitation phenomena and their possibly adverse biological effects has produced a significant amount of information on cavitation thresholds. Robert Apfel's studies of pulsed ultrasound cavitation effects [Ref. 3] have summarized the possible biological effects in single cells due to excessive sound pressure amplitudes. His work has accounted for the effects of frequency, liquid inertia, and fluid viscosity in the cavitation process. H. G. Flynn has done extensive numerical modelling of cavitation phenomena, also taking into account viscosity and surface tension as well as compressibility and heat conduction [Ref. 4]. R. A. Roy, *et al.* [Ref. 5], and A. A. Atchley, *et al.* [Ref. 6], have produced precision techniques for measuring transient acoustic cavitation thresholds by detecting the light and sound emissions produced during violent bubble collapse. It is their research that has become the basis for the research reported in this thesis. Although some aspects of cavitation thresholds have been previously investigated, there has been little work done to determine the time evolution of the cavitation event. The objectives of this research are to (1) develop an apparatus in which cavitation can be induced and detected simultaneously by two methods—acoustic scattering and sonoluminescence; (2) determine transient cavitation thresholds; and (3) examine the time evolution of the transient cavitation events.

II. THEORY

A. BACKGROUND

The behavior of bubbles under the influence of an acoustic pressure field is indeed complex. In this study, we will examine the pressure amplitudes of pulsed ultrasound which will induce the rapid growth and collapse of cavitation nuclei. We will vary the frequency of the acoustic signal, the number of acoustic cycles per pulse, and the rest time between pulses in order to more fully understand the effects of each parameter on the pressure amplitude required to cause the nuclei to behave in this manner. In addition, we will develop an apparatus that provides for both acoustic and optical observation of the cavitation events. We must therefore be aware not only of the behavior of the bubbles when influenced by the sound field but also of their propensity for scattering sound and producing visible light.

In this chapter, we will review the above-mentioned aspects of bubble behavior. We will first look at the three regimes of acoustic cavitation: stable cavitation, transient cavitation, and gas body activation. We will describe the theory that describes bubble activity under static equilibrium conditions, under the influence of a continuous sound pressure field in which controlled bubble oscillations occur, under conditions which result in controlled growth of the bubbles, and under conditions which lead to unstable growth and violent collapse. A theory will be described that allows one to predict the peak acoustic pressure which produces the collapse of a gas bubble. Finally, we will

examine the theories which explain both light emission (sonoluminescence) upon bubble collapse and acoustic scattering from multiple bubbles.

B. CAVITATION REGIMES

It is generally acknowledged that two, and possibly three, cavitation regimes exist. The focus of our research will be transient cavitation produced by pulsed ultrasound. As the name indicates, this regime is transient in nature; bubbles are likely to exist for less than a few acoustic cycles. The results of the measurements to be described later indicate that effects of the second regime, stable cavitation, may also be important. Stable cavitation occurs when a bubble subjected to a sound field oscillates about its equilibrium radius. This regime is characterized by bubbles that are relatively permanent; noticeable changes in the equilibrium radius occur only after many cycles. The third regime (considered by many not to be a true cavitation regime) is known as gas body activation, which involves the oscillations of gas pockets permanently embedded in cracks, crevices, or within biological systems. As gas body activation does not include actual formation and growth of gas bubbles, only stable and transient cavitation will be discused further in this chapter.

C. BUBBLES UNDER QUASI-STATIC EQUILIBRIUM CONDITIONS

The first stage of any cavitation problem is nucleation, or the formation of a macroscopically observable bubble from a cavitation nucleus. This formation usually involves the loss of mechanical

stability of the nucleus. Following the developments of Walton and Reynolds [Ref. 7], Noltingk and Neppiras [Ref. 8], and Blake [Ref. 9], a brief examination will be made of the conditions required for a spherical bubble to lose its static equilibrium in a liquid.

Given a bubble of radius R_0 in static equilibrium with a liquid of infinite extent at a hydrostatic pressure P_0, the pressure inside the bubble is given by

$$P = P_0 + \left(\frac{2\sigma}{R_0}\right). \tag{2.1}$$

The term $\left(\frac{2\sigma}{R_0}\right)$ is known as the Laplace or Young pressure and is due to the surface tension of the liquid, σ (the usually minor contribution of the vapor pressure has been neglected). Assuming that the liquid undergoes an incremental change in hydrostatic pressure to a new value P_∞, the bubble radius will undergo an incremental change to some new radius R. Assuming isothermal conditions and an ideal gas, we note

$$P_1V_1 = P_2V_2 = \text{constant}$$

where

$$P_1V_1 = \left(P_0 + \frac{2\sigma}{R_0}\right)\frac{4}{3}\pi R_0^3$$

and

$$P_2V_2 = \left(P_\infty + \frac{2\sigma}{R}\right)\frac{4}{3}\pi R^3.$$

The assumption of isothermal conditions is justified because the rate of evaporation and condensation of vapor at the bubble surface is sufficient to maintain this condition. After combining these two expressions and cancelling common terms, we find that

$$P_\infty = \left(P_0 + \frac{2\sigma}{R_0}\right)\left(\frac{R_0}{R}\right)^3 - \frac{2\sigma}{R}. \qquad (2.2)$$

Figure 2.1, which is a plot of P_∞ as a function of R, offers insight into the stability of bubbles. Assuming there is no gas diffusion into or out of a bubble, P_∞ is the value of the liquid pressure necessary to balance the sum of the internal pressure (which tends to make the bubble expand) and the Laplace pressure (which makes the bubble collapse). P_∞ is a minimum for a bubble of radius R^*. Bubbles of radius less than R^* are in stable equilibrium, whereas bubbles of radius greater than R^* are in unstable equilibrium. To see this more clearly, consider a bubble of radius $R<R^*$. If R is increased, P_∞ decreases because the decrease in the Laplace pressure $\left(\frac{2\sigma}{R}\right)$ is less than the decrease in internal pressure. Consequently, the external liquid pressure needed to maintain equilibrium is now less than the actual external pressure. As a result, the bubble shrinks back to R. In other words, the collapsing pressure dominates over the

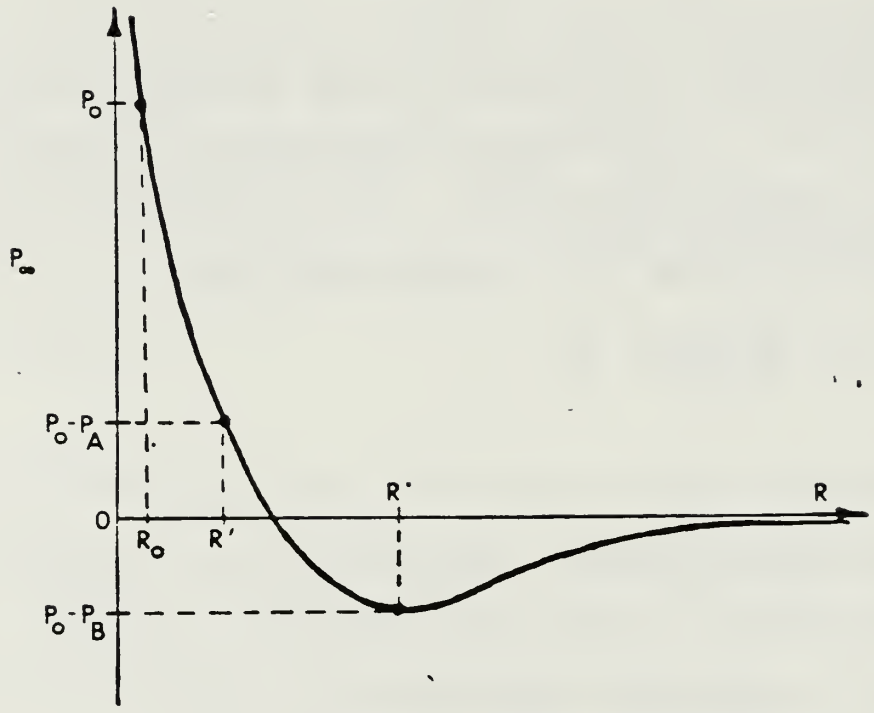

Figure 2.1

Graph of Pressure vs. Bubble Radius Showing Stable and Unstable Equilibrium States of Bubbles Within a Liquid (from [Ref. 7]

expanding pressure. If the radius had been made smaller, P_∞ would increase corresponding to a dominance of the expanding pressure. Again, the bubble returns to R. Therefore, the bubble is in a state of stable equilibrium—perturbations in the radius cause the bubble to return to its initial radius. By invoking a similar argument for bubbles of radius greater than R^*, it is seen that the equilibrium is unstable. An increase in radius causes P_∞ to increase due to the dominance of the expanding pressure. The bubble would increase in size

indefinitely. A decrease in radius causes the bubble to shrink to the corresponding stable value of R. Because of its role in determining the stability of bubbles, R^* is called the critical radius.

Now, consider a bubble of radius $R_0 < R^*$ in equilibrium at pressure P_0. According to Figure 2.1, it is stable. If the pressure is lowered to some value $P_0 - P_A$, the bubble will grow until it reaches a new stable equilibrium radius R' (since $R' < R^*$). If, however, the pressure is reduced to $P_0 - P_B$, where P_B is the Blake threshold pressure, the bubble reaches the critical radius R^*. Any further reduction in pressure provides no equilibrium value for the bubble radius, and the bubble grows uncontrollably. To solve for R^*, we must minimize P_∞ as a function of radius.

Rewriting equation (2.2) slightly,

$$P_\infty = \left(P_0 + \frac{2\sigma}{R_0}\right) R_0^3 \cdot \left(\frac{1}{R^3}\right) - \frac{2\sigma}{R}, \tag{2.3}$$

then differentiating with respect to R and setting the result equal to zero, we find

$$R^* = \left[\frac{3\left(P_0 + \frac{2\sigma}{R_0}\right)R_0^3}{2\sigma}\right]^{1/2}. \tag{2.4}$$

Previously, we considered the Blake Pressure to be a function of initial bubble radius. The converse view is to consider the initial radius to be a function of Blake pressure. Accordingly, the Blake

radius R_B is the initial radius of a bubble that, when subjected to the (acoustic) Blake pressure P_B, grows to a radius of R^*, becomes unstable, and grows uncontrollably. To find the Blake threshold pressure, we first rewrite R^* (equation 2.4) in terms of R_B:

$$R^* = \left[\frac{3\left(P_0 + \frac{2\sigma}{R_B}\right)R_B^3}{2\sigma} \right]^{1/2} . \tag{2.5}$$

Letting

$$K = \left(P_0 + \frac{2\sigma}{R_B}\right)R_B^3 \tag{2.6}$$

allows R^* to be expressed more simply as

$$R^* = \left(\frac{3K}{2\sigma}\right)^{1/2} , \tag{2.7}$$

or

$$\frac{K}{R^{*2}} = \frac{2\sigma}{3} \tag{2.8}$$

Setting $R_0 = R_B$, $R = R^*$, and $P_\infty = P_0 - P_B$ in equation (2.3), we find

$$P_\infty = P_0 - P_B = \frac{2\sigma}{3R^*} - \frac{2\sigma}{R^*} , \tag{2.9}$$

or

$$P_0 - P_B = -\frac{4}{3}\frac{\sigma}{R^*} . \tag{2.10}$$

Rewriting this expression using equations (2.7) and (2.6), we find

$$P_0 - P_B = -\frac{8}{9}\sigma\left[\frac{3\sigma}{2(P_0 + \frac{2\sigma}{R_B}R_B^3)}\right]^{1/2}, \qquad (2.11)$$

which can be written in normalized form as

$$p_b = \frac{P_B}{P_0} = 1 + \frac{4}{9}X_B\left[\frac{3X_B}{4(1 - X_B)}\right]^{1/2} \qquad (2.12)$$

where $X_B = \frac{2\sigma}{R_0P_0}$.

Summarizing this discussion, a bubble of radius R_B in stable equilibrium will lose its stability if subjected to an acoustic pressure of amplitude P_B. Upon loss of stability, the bubble will expand to many times its initial size; i.e., it will form a macroscopically observable bubble.

D. BUBBLES UNDER THE INFLUENCE OF A SOUND FIELD

We begin the examination of bubble motion under the influence of a sound field with a description of bubble motion by Rayleigh [Ref. 10]. He initially considered the collapse of an empty spherical cavity located in an infinite mass of incompressible fluid. The hydrostatic pressure in the liquid is assumed constant. Rayleigh observed that the work done by the collapsing bubble starting from rest had to be equal to the kinetic energy of the fluid. Thus, the following holds true:

$$P_\infty \frac{4\pi}{3}(R_0^3 - R^3) = \frac{1}{2}\rho\int_R^\infty v^2(r)\ 4\pi r^2 dr \qquad (2.13)$$

where r is the distance from the center of the bubble to a point in the liquid that is greater than the radius of the bubble R and v(r) is the velocity of the fluid. P_∞ is the hydrostatic pressure of the liquid and $\frac{4\pi}{3}\left(R_0^3 - R^3\right)$ is the decrease in volume of the spherical cavity. The right-hand term is the kinetic energy of the liquid, $\frac{1}{2}mv^2$. Since the fluid is incompressible, the change in volume of the liquid is equal to the change in volume of the bubble and the following relationship is true:

$$4\pi r^2 v(r) = \text{constant.}$$

Therefore, $4\pi r^2 v(r) = 4\pi R^2 v(R)$ or $v^2(r) = \frac{R^4}{r^4} v^2(R)$. Letting $v(R) = \dot{R}$, it can be shown that

$$v^2 = \frac{R^4 \dot{R}^2}{r^4}. \tag{2.14}$$

Substituting this result into equation (2.13) and performing the integration on the right-hand side yields

$$P_\infty \frac{4\pi}{3}(R_0^3 - R^3) = 2\pi \rho R^3 \dot{R}^2 . \tag{2.15}$$

Solving for $\dot{R}^2$:

$$\dot{R}^2 = \frac{2}{3\rho} P_\infty \left(\frac{R_0^3}{R^3} - 1\right). \tag{2.16}$$

Since $\dot{R}$ is equal to $\frac{dR}{dt}$, it is apparent that $dt = \frac{dR}{\dot{R}}$. As R decreases, however, $\dot{R}$ is compelled to approach infinity. At this point, Rayleigh strives to avoid this obvious flaw by admitting that the initial assumption of zero internal pressure is invalid. He then assumes that the cavity is filled with a perfect gas undergoing an isothermal compression. If this assumption is true, Boyle's law holds and the pressure within the bubble will increase until the bubble begins to rebound. If fluid viscosity is zero and all other losses ignored, the bubble will continue to oscillate between this minimum radius and the initial radius R_0. Again invoking the assumption that initial pressure inside the bubble is zero or at least some constant, Rayleigh has derived the following equation governing pressure within the liquid, p, at any point:

$$\frac{p}{P_\infty} - 1 = \frac{R}{3r}\left(\frac{R_0^3}{R^3} - 4\right) - \frac{R^4}{3r^4}\left(\frac{R_0^3}{R^3} - 1\right). \qquad (2.17)$$

The work of Plesset, Poritsky, and Noltingk and Neppiras contributed to the final formulation of an equation that describes the motion of a bubble under the influence of an acoustic field. Plesset [Ref. 11] extended Rayleigh's analysis, as did Poritsky [Ref. 12] and Noltingk and Neppiras [Ref. 13]. In 1976, Lauterborn [Ref. 14] combined these results with previously described results to form the final characteristic equation governing bubble motion, the RPNNP equation.

Lauterborn so named this equation in honor of the pioneering work done by Rayleigh, Plesset, Noltingk, Neppiras, and Poritsky. In review, he set the work done by the liquid at infinity minus the work done by the liquid layer immediately adjacent to the bubble equal to the kinetic energy of the liquid surrounding the bubble:

$$\int_{R_0}^{R} (P_L - P_\infty)\, 4\pi r^2\, dr = 2\pi\rho R^3 \dot{R}^2. \tag{2.18}$$

where P_L is the pressure in the liquid layer immediately surrounding the bubble. The reader should note that P_∞ in this development is varying with time:

$$P_\infty = P_0 + P(t)$$

where P_0 is a static pressure about which P(t) varies. Therefore, from Reference 14, P_L can be expressed as

$$P_L = \left(P_0 + \frac{2\sigma}{R_0} - P_V\right)\left(\frac{R_0}{R}\right)^{3\kappa} - 2\,\frac{\sigma}{R} - 4\mu\,\frac{\dot{R}}{R} \tag{2.19}$$

where κ is the polytropic exponent of the gas inside the bubble, μ is the shear viscosity of the liquid, and P_v is its vapor pressure. Differentiating (2.18) and substituting (2.19) for P_L and $P_\infty = P_0 + P(t)$, we find that

$$R\ddot{R} + \frac{3}{2}\dot{R}^2 = \frac{1}{\rho}\left[\left(P_0 + \frac{2\sigma}{R_0} - P_V\right)\left(\frac{R_0}{R}\right)^{3\kappa} - \frac{2\sigma}{R} - \frac{4\mu\dot{R}}{R} - P_0 - P(t)\right]. \tag{2.20}$$

The following assumptions are implicit in this comprehensive equation [Ref. 7]:

1. The bubble remains spherical at all times;
2. Uniform conditions exist within the bubble;
3. The acoustic wavelength, λ, is much greater than R;
4. No body forces are present;
5. Bulk viscosity is ignored;
6. The liquid is incompressible;
7. Gas content of the bubble is constant— no diffusion occurs;
8. Vapor pressure, P_V, is constant during the bubble's motion.

Although many simplifying assumptions have been made in deriving equation (2.20), it is a better-than-reasonable description of the dynamics of a bubble subjected to an ultrasonic sound field [Ref. 7]. In addition, the RPNNP, or simply the Rayleigh-Plesset, equation is the foundation of the theories discussed in the next two sections.

E. STABLE BUBBLE GROWTH DUE TO AN ACOUSTIC PRESSURE FIELD

Stable cavitation and rectified diffusion, although neglected in the RPNNP equation, are two related and interesting processes which may be important in the time evolution of transient cavitation events. The stable growth of cavitation nuclei to sizes which allow transient growth is a likely mechanism for producing transient cavitation. Rather than undertake a rigorous mathematical development of rectified diffusion

as in Reference 15, a qualitative description of this phenomenon will be presented here.

The importance of rectified diffusion, or incremental enlargement, was first noted by Harvey, et al., in 1944 [Ref. 16]. Blake [Ref. 9] was the first to attempt the derivation of a mathematical model in 1949. Two effects, the area effect and the shell effect, appear to work in concert to produce bubble growth.

1. The Area Effect

When a bubble contracts, the concentration of gas within the bubble increases. Since gas diffuses from regions of high concentration to those of low concentration, the gas diffuses out of the bubble. When the bubble expands, the concentration of gas decreases, and the concentration gradient reverses, the result being a diffusion of gas into the bubble. The diffusion rate is proportional to the area through which gas may flow. Therefore, more gas enters the bubble when it is expanded than leaves when it is contracted. The net result is an influx of gas during one complete oscillation of the bubble.

2. The Shell Effect

The rate of diffusion, as noted above, is proportional to the concentration gradient. Crum [Ref. 15] considers a spherical shell of liquid surrounding a bubble. He argues that, when the bubble contracts, the shell expands, with a consequent reduction in gas concentration near the bubble surface. This increases the concentration gradient in the outward direction over that discussed above, so the diffusion of gas out of the bubble is even greater. Conversely, when the bubble expands,

the shell volume decreases, the gas concentration increases, and the concentration gradient into the bubble increases. The overall result is the enhancement of the area effect.

3. Threshold Equation

There exist both high- and low-frequency thresholds for rectified diffusion. Crum has formulated expressions for both. Of interest here is the high-frequency approximation [Ref. 15]:

$$P_A^2 = \frac{\left(\rho R_0^2 \omega_0^2\right)\left[\left(1 - \frac{\omega^2}{\omega_0^2}\right)^2 + b^2\right]\left[1 + \frac{2\sigma}{R_0 P_\infty} - \frac{C_1}{C_0}\right]}{(3+4K)\left(\frac{C_1}{C_0}\right) - K\left(1 + \frac{2\sigma}{R_0 P_\infty}\right)} \qquad (2.21)$$

where

P_A = pressure threshold for rectified diffusion

$$K = \frac{\left[\left(1 - \frac{\beta^2}{4}\right) + \frac{5\sigma}{3 P_\infty R_0}\right]}{\left[1 + \left(\frac{4\sigma}{3 P_\infty R_0}\right)\right]}$$

$\beta^2 = \rho \omega^2 R_0^2 / 3 P_\infty$

$b = 4\omega\mu / 3 P_\infty$ (Damping term)

$\omega_0^2 = \left(\frac{1}{\rho R_0^2}\right)\left(3 P_\infty + \frac{4\sigma}{R_0}\right)$ (small amplitude resonance frequency squared)

C_0 = equilibrium concentration of gas in the liquid

C_i = concentration of dissolved gas in the liquid far from the bubble

μ = viscosity of the liquid

ω = angular frequency of the acoustic field

R_0 = equilibrium bubble radius

ρ = liquid density

P_∞ = ambient pressure

σ = surface tension of the liquid

F. BUBBLES DRIVEN TO UNSTABLE GROWTH AND VIOLENT COLLAPSE

The final step in development of the theory which defines bubble behavior in a sound field is taken from research by R. A. Apfel and H. G. Flynn. In Reference 3, Apfel indicates that the possibly adverse biological effects of acoustics are linked to the growth and collapse of submicron cavitation nuclei. A nucleus "that grows to 5 μm in one acoustic cycle will, upon collapse, deposit in the size scale of one biological cell approximately 300 million electron volts (MeV)" of energy [Ref. 3]. This energy, in the form of heat, results in internal gas temperatures in the range of 1000–5000 K. At such high temperatures, effects such as free radical formation and recombination can occur. These effects can result in the production of visible light that can be detected optically (this will be discussed in detail later in this

chapter). Apfel's work culminates in a formula that predicts the peak acoustic pressure which produces a cavitation event (collapse) given the initial bubble radius R_0 and maximum internal gas temperature 5000 K with acoustic frequency, density, viscosity, and surface tension of the liquid as parameters. He develops the relationship between the maximum collapse temperature T' and normalized acoustic pressure p = $\frac{P_A}{P_0}$ (P_A is peak acoustic pressure; P_0 is ambient pressure) by relating p to R_{max} (maximum bubble radius) and R_{max} to T'. Although a rigorous development of these two relations will not be conducted here, Figure 2.2 shows readily how bubble size corresponds to applied acoustic pressure. The reader is referred to Reference 2 for a more rigorous development of T' vs. R_{max} and R_{max} vs. p. It is necessary, however, to examine Figure 2.2 carefully to determine the character of the R_{max} vs. p relationship. The maximum bubble radius can be thought of as being composed of two parts: R_1, which occurs when ΔP, the pressure difference across the bubble, is negative (outward force); and R_{max}, which occurs when ΔP is positive, yet the bubble continues to expand due to outward liquid momentum.

The time over which maximum bubble radius is computed is also noted in Figure 2.2. The time τ, during which ΔP is negative, is the algebraic sum of t_2, t_1, and Δt.

$$\tau = t_2 - t_1 - \Delta t, \qquad (2.22)$$

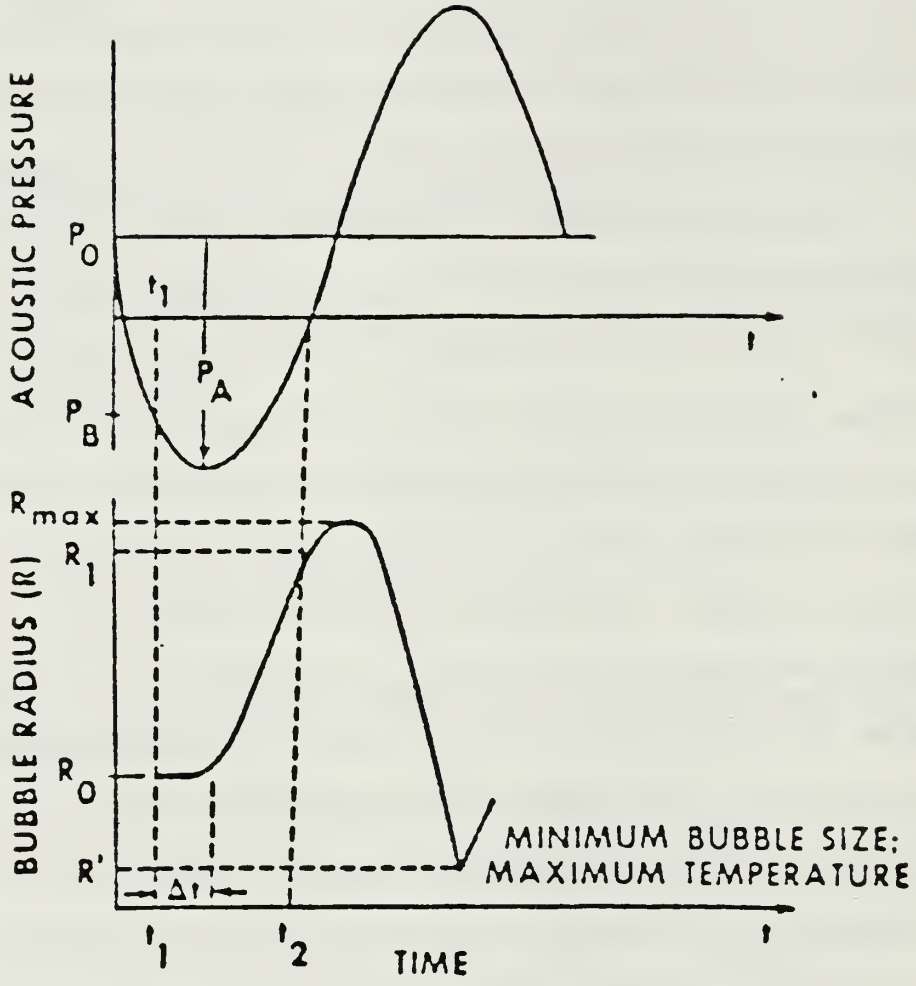

Figure 2.2

Schematic of Bubble Radius as a Function of Time When Subjected to a Single Acoustic Cycle (from [Ref. 3])

where

$$t_2 \equiv \frac{1}{\omega}\left[\frac{\pi}{2} + \sqrt{\frac{2(p-1)}{p}}\right], \tag{2.23}$$

$$t_1 \equiv \frac{1}{\omega}\left[\frac{\pi}{2} + \sqrt{\frac{2(p-p_b)}{p}}\right], \tag{2.24}$$

and

$$\Delta t \cong \frac{2}{3} R_0 \sqrt{\frac{\rho}{\Delta P}} + \frac{4\mu}{\Delta P}, \tag{2.25}$$

where $p = \frac{P_A}{P_0}$ and p_b is the normalized Blake threshold pressure given by equation (2.12). The value of τ is therefore

$$\tau = \frac{1}{2\pi f}\left[\sqrt{\frac{2(p-1)}{p}} - \sqrt{\frac{2(p-p_b)}{p}}\right] - \frac{2}{3} R_0 \sqrt{\frac{\rho}{\frac{2}{3} P_0 (p-1)}} - \frac{6\mu}{P_0 (p-1)} \tag{2.26}$$

The maximum bubble radius can now be estimated by

$$R_{max} \cong \left[R_0 + \frac{2}{3}\sqrt{\frac{P_0(p-1)}{\rho}}\tau\right]\left[1 + \frac{2}{3}(p-1)\right]^{1/3} \tag{2.27}$$

From the perfect gas law, $\frac{PR^3}{T}$ = constant, and its adiabatic form $PR^{3\gamma}$ = constant, it can be shown that

$$T' = T_0 (\gamma - 1)\left(\frac{R_{max}}{R_0}\right)^3. \tag{2.28}$$

From equations (2.26) and (2.27), above, we find

$$T' = T_0 (\gamma - 1)\left[1 + \frac{2}{3} R_0^{-1}\sqrt{\frac{P_0 (p-1)}{\rho}}\tau\right]^3 \cdot \left[1 + \frac{2}{3}(p-1)\right] \tag{2.29}$$

It is now convenient to find frequency (embedded in τ), resulting in:

$$f = \frac{\frac{1}{3\pi R_0}\sqrt{\frac{P_0\,\chi}{\rho}}\left[\sqrt{\frac{(p-1)}{p}}+\sqrt{\frac{(p-p_b)}{p}}\right]}{\frac{3.46}{\left[\frac{\chi}{3}+1\right]^{1/3}}+\frac{4\mu}{R_0}\sqrt{\frac{2}{\rho\,P_0\,\chi}}-0.46}, \qquad (2.30)$$

where

$$\chi = p_b + p - 2 + \sqrt{(p-1)\,(p-p_b)}.$$

In Table 2.1 from Reference 3 and Figure 2.3 from Reference 4, the effects of initial bubble radius and frequency in transient cavitation threshold can be seen. It is important to note that frequency and internal temperature have little effect on the threshold pressures of smaller bubbles, but become increasingly important as initial bubble radius gets larger. This approximate formulation is not meant to be a substitute for more exact numerical calculations such as are found in Reference 4, but it does give a reasonable idea of the manner in which the parameters of frequency, viscosity, and initial bubble radius affect the transient cavitation threshold of a liquid.

G. SONOLUMINESCENCE

Since one of the goals of this thesis is to develop both optical and acoustical cavitation detection schemes, it is important to present some theories concerning sonoluminescence. Following the review of Walton and Reynolds [Ref. 7], two primary theories as to the origin of sonoluminescence have been advanced.

TABLE 2.1

PRESSURE THRESHOLDS PREDICTED BY EQUATION (2.30)

T° K.	f(MHz)	Pressure (bar) $R_0 = 0.1$ μm	Pressure (bar) $R_0 = 0.5$ μm
2500	1.0	6.4	2.0
5000		6.4	2.1
2500	2.5	6.4	2.8
5000		6.4	3.1
2500	5.0	6.4	4.2
5000		6.4	5.1

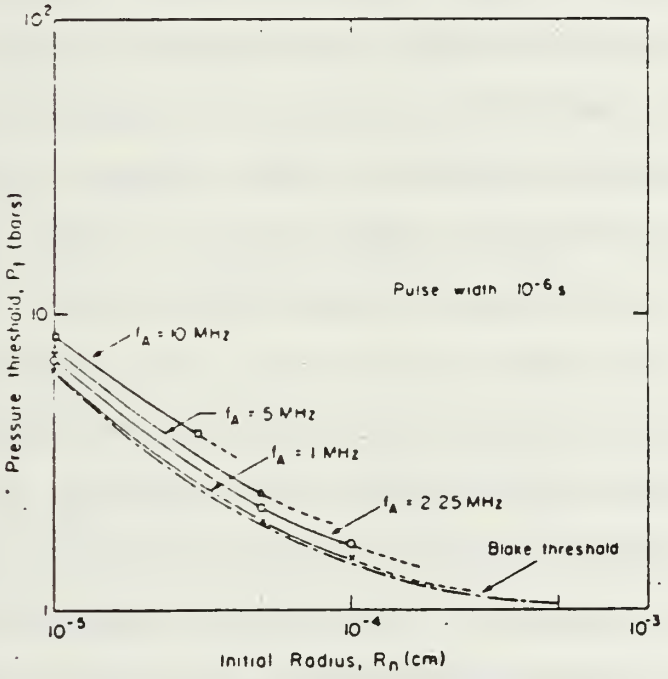

Figure 2.3

Threshold Pressure P_t (in Bars) for Transient Cavitation as a Function of Initial Radius R_0 Over a Range of Frequency f_A at a Pulse Width of 1μs [Ref. 4]

Noltingk and Neppiras [Ref. 13] proposed that sonoluminescence is the result of black-body radiation from the gas contained within the bubble, which theoretically rises to extreme temperatures as the bubble undergoes a rapid adiabatic compression during its collapse.

Griffing [Ref. 17] proposed that the formation of highly reactive free radials in the liquid during bubble collapse were responsible for rapid chemical changes in the fluid, resulting in the emission of light.

For the most recent examinations of sonoluminescence, the interested reader is referred to References 18 through 22. The preponderance of evidence points to the formation of free radicals that subsequently play a role in sonoluminescence. These free radicals, or "reactive molecules (or atoms) with unpaired electrons" [Ref. 23] may be formed as a result of the dissociation of molecules subjected to the high temperatures produced by a rapid adiabatic compression. Often, if a free radical (with its unpaired electron) reacts with a molecule having its full complement of paired electrons, the result is another free radical. This chain of events will be self-sustaining until all of the suitable material has been reacted with, the free radicals have combined with each other to form stable molecules, or all of the free radicals have collided with the wall of the container, where they are removed from the process. According to Griffing, the emission of light may be due to one of these free radical reactions that happens to be of a chemiluminescent nature. This hypothesis has been confirmed by a number of subsequent experiments [Refs. 18-22].

H. ACOUSTIC SCATTERING FROM BUBBLES

The other detection method that we hope to use to investigate transient cavitation is the scattering of an acoustic signal (either the source signal or an alternate lower-frequency active signal) from bubbles generated by such events. This technique is expected to take advantage of the exceptionally large scattering cross-section of resonant bubbles. Since our measurements do not require numerical solution of scattering parameters, however, a qualitative explanation rather than a rigorous mathematical development will be given here. This theory is taken from Clay and Medwin [Ref. 24].

A small, rigid sphere whose density and elasticity are greater than that of the medium backscatters a very small amount of the acoustic energy when ensonified by acoustic frequencies where the wavelength is much greater than the sphere's radius. The acoustical cross-section of the sphere is, in fact, much smaller than the geometrical cross-section because of diffraction of the incident sound field around the small, rigid body.

Bubbles, however, differ from rigid spheres in two ways: (1) the specific acoustic impedance (ρc) of the gas within the bubble is much less than that of the water, and (2) bubbles resonate. Bubbles are extremely effective absorbers and scatterers of sound at frequencies near resonance frequencies. Scattering cross-sections at resonance are on the order of 400 times their geometrical cross-sections. (See Figure 2.4.)

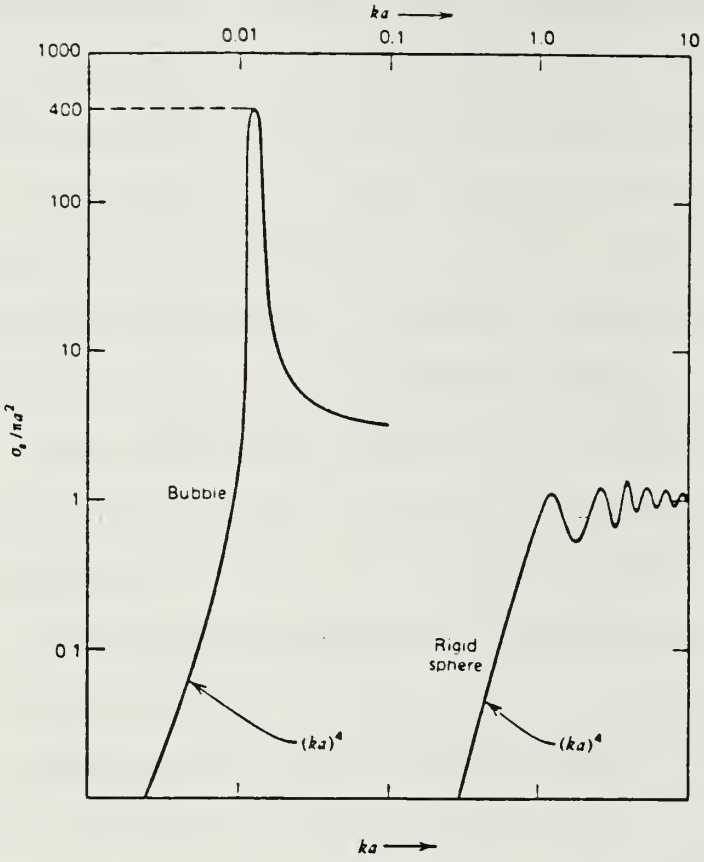

Figure 2.4

Ratio of Scattering Cross-Section to Geometrical Cross-Section for a Bubble and a Rigid Sphere (from [Ref. 24])

Transient cavitation events studied in this investigation will result in the generation of many bubbles of varying sizes. The effects of multiple scattering must be considered. When scatterers are widely spaced, the scattering cross-section per unit volume is simply the sum of the individual scattering cross-sections of the bubbles within

that volume. The bubble "cloud" expected as a result of the transient cavitation event will be much more densely packed, however, which will cause the individual scattered fields of the oscillating bubbles to interact. The result is that the resonance curve of a single bubble shown in Figure 2.4 is broadened and the scattering cross-section of an array of bubbles is less than the sum of the individual cross-sections. A cloud of bubbles—bubbles packed randomly in a three-dimensional array—acts as a pressure release surface at the face of the cluster, thus reflecting acoustic energy at this interface. It is this effect that is expected to reveal the presence of acoustic cavitation.

III. EXPERIMENTAL APPARATUS

A. BACKGROUND

The apparatus with which these cavitation measurements will be made is based upon a system developed by A. A. Atchley, L. A. Frizzell, and R. E. Apfel [Ref. 6]. Our apparatus differs from theirs in three major areas: (1) cavitation detection can be accomplished by two methods: optically (via sonoluminescence) and acoustically, either individually or simultaneously; (2) this apparatus will rely on random bubble nuclei attaining threshold radii vice providing an artificially introduced uniform cavitation nucleus to the sound field; and (3) this apparatus is computer-controlled. The system is made up of two major subsystems: the fluid management system and the electronics system. The fluid management system will distill, filter, and degas ordinary tap water for use in the cavitation enclosure. The electronics system will provide the capability to induce, detect, and record transient cavitation events, all under computer control.

B. CAVITATION ENCLOSURE AND LIGHT-TIGHT ENCLOSURE

The cavitation enclosure (Figure 3.1) is a 25 cm by 15 cm by 15 cm box made of 1.2 cm thick plexiglass. Plexiglass was chosen as the primary structural material because it is sufficiently strong to support installed transducers and fluid inlet and outlet connections, yet it allows the optical detection apparatus to "see" what occurs in the insonified region of the system. One end of the chamber holds a

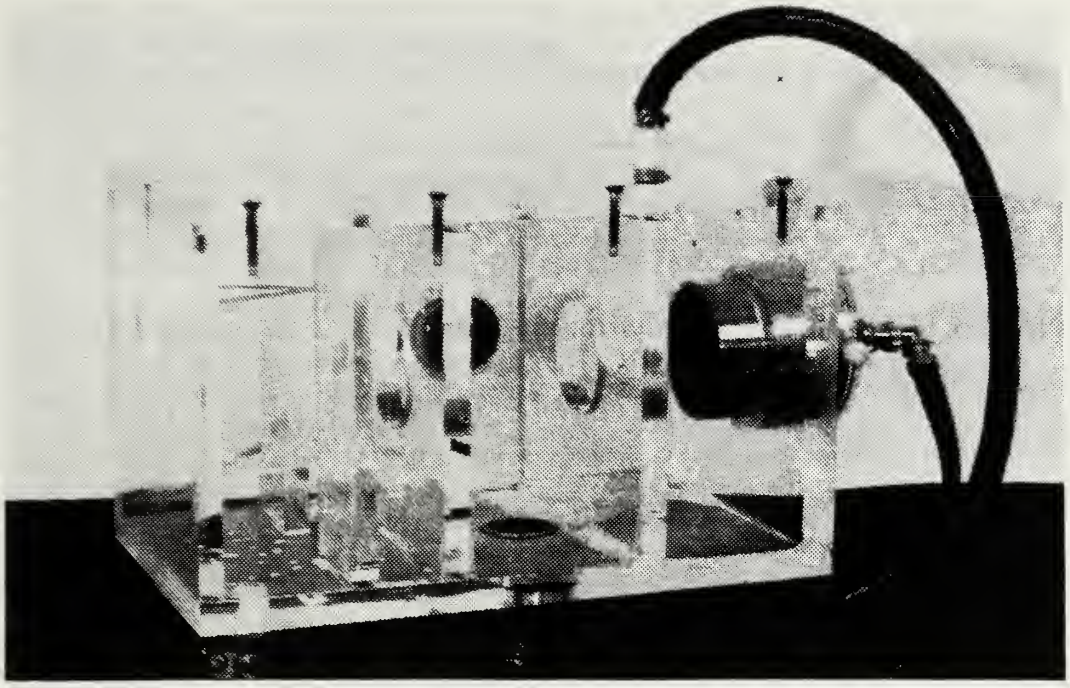

Figure 3.1

Cavitation Enclosure

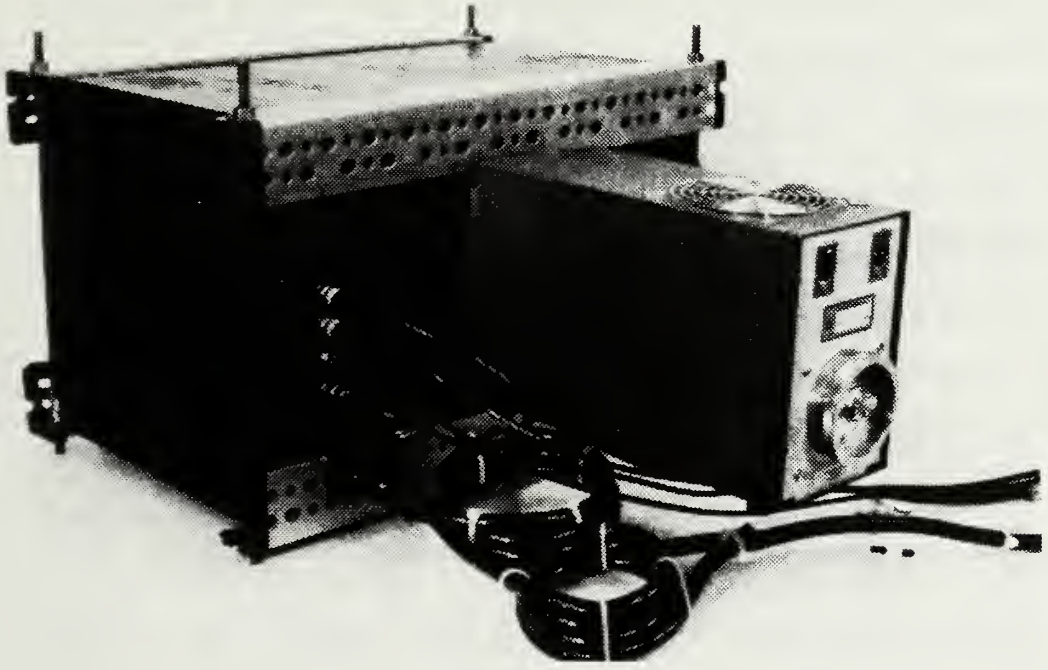

Figure 3.2

Light-Tight Enclosure and Photomultiplier Tube Assembly

Harisonic Labs focused transducer that supplies the cavitation generation signal. A wedge and two vertical walls (also plexiglass) have been installed at the opposite end of the enclosure to scatter the incident sound and thus minimize reflections that would interfere at the focal region. The source transducers (rated at 1.0 MHz and 2.25 MHz) have focal lengths of 7.6 cm. Two additional walls with holes cut to allow passage of the focused sound beam are installed on either side of the focal region, again to minimize interference from reflections. The mounting for the source transducer allows for rapid changing of elements so that the other source frequency can be examined. Two Panametrics V301 transducers are permanently installed in the bottom and one side of the enclosure in such a manner that their beam pattern intersects the focal region of the source transducer. The top of the enclosure is removable to allow access to the interior. The cavitation enclosure is placed in a light-tight box that has connections for fluid inlet and outlet as well as BNC connections for source and receive transducer signals (Figure 3.2). The photomultiplier tube (PMT) assembly is mounted on one side of the light-tight enclosure so that it also can "see" the focal region for sonoluminescent indications of cavitation. The photomultiplier tube's sensitive circuitry is protected by a mechanical shutter that can be lowered to block light and by an interlock switch in the lid of the enclosure that interrupts the high-voltage power supply to the PMT when the lid is removed.

C. FLUID MANAGEMENT SYSTEM

The fluid management system (Figure 3.3) consists of a four-element deionization/filtration system, a bag-type 0.2 μm filter, a small variable-speed electric centrifugal pump, an ultraviolet sterilizer, and an Erlenmeyer flask with connections for system evacuation and argon infusion. The Erlenmeyer flask is also used as a fluid reservoir and expansion tank. The filtration/deionization system produces the equivalent of quintuply distilled water and removes all ionized minerals, silicon, and free carbon dioxide down to four parts per billion. The bag filter ensures that no particles larger than 0.2 μm are introduced into the system. These two elements are used only when the system is being filled. When the system is fully charged, the water is circulated through the cavitation enclosure via a closed loop consisting of the pump, the U/V sterilizer, the enclosure, and the expansion reservoir. Argon is bubbled into the fluid to help enhance the sonoluminescent reaction. The system is simultaneously evacuated (15 inches Hg vacuum) in order to remove dissolved gases. The evacuation is continued until visible air bubbles are removed (usually about one hour). The circulation system is then secured and the sample is returned to atmospheric pressure, where it remains quiescent for one-half hour before data accumulation begins. After about an hour of data accumulation (usually 20 to 40 data points), the system must be drained, refilled, and reprocessed. Refilling the system is necessary because the fluid becomes "tired" after multiple cavitation events, causing higher-than-normal thresholds (possibly due to fewer remaining cavitation nuclei).

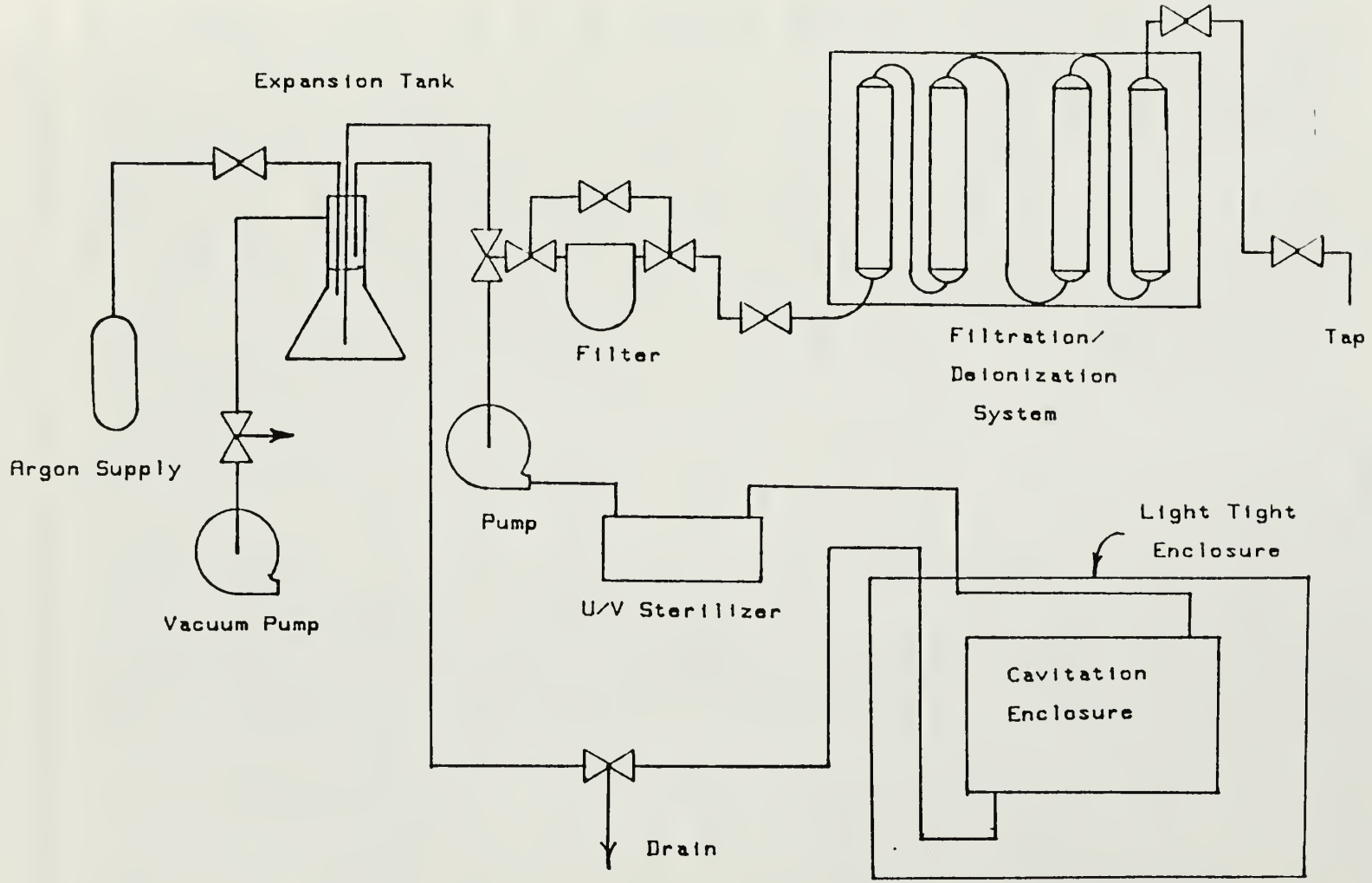

Figure 3.3

Fluid Management System

D. CAVITATION GENERATION AND DETECTION SYSTEM

The electronics system consists of the cavitation generation system and the cavitation detection system (Figure 3.4). The heart of the cavitation generation system is the Hewlett-Packard 9000 Series 300 personal computer, which controls the output frequency, pulse width (duty cycle), pulse repetition rate, and acoustic pressure amplitude of the source transducer via the Hewlett-Packard 3314A function generator. The output of the function generator is boosted by an Amplifier Research 100-A15 Power Amplifier and is then applied to the source transducer. A printout of the control program is contained in Appendix A.

The cavitation detection system consists of two subsystems: the acoustic detection system and the photomultiplier tube (PMT) assembly. The acoustic detection system is made up of the two Panametrics V301 transducers installed in the cavitation enclosure and the associated elements for either passive or active (via scattering of a cw signal) detection of cavitation events. In the passive mode, the output of one of the detection transducers is boosted by a small RF amplifier and is displayed on the Tektronix 2245A oscilloscope. The trace of this signal on the oscilloscope consists primarily of a bundle of acoustic pulses that have either been diffracted or scattered to the detection transducer face. The bundle is delayed from the source pulse by approximately 100 microseconds, which corresponds to the time the pulse would take to make the 15 cm journey from the source to the focal region and then to the detection transducer face. The

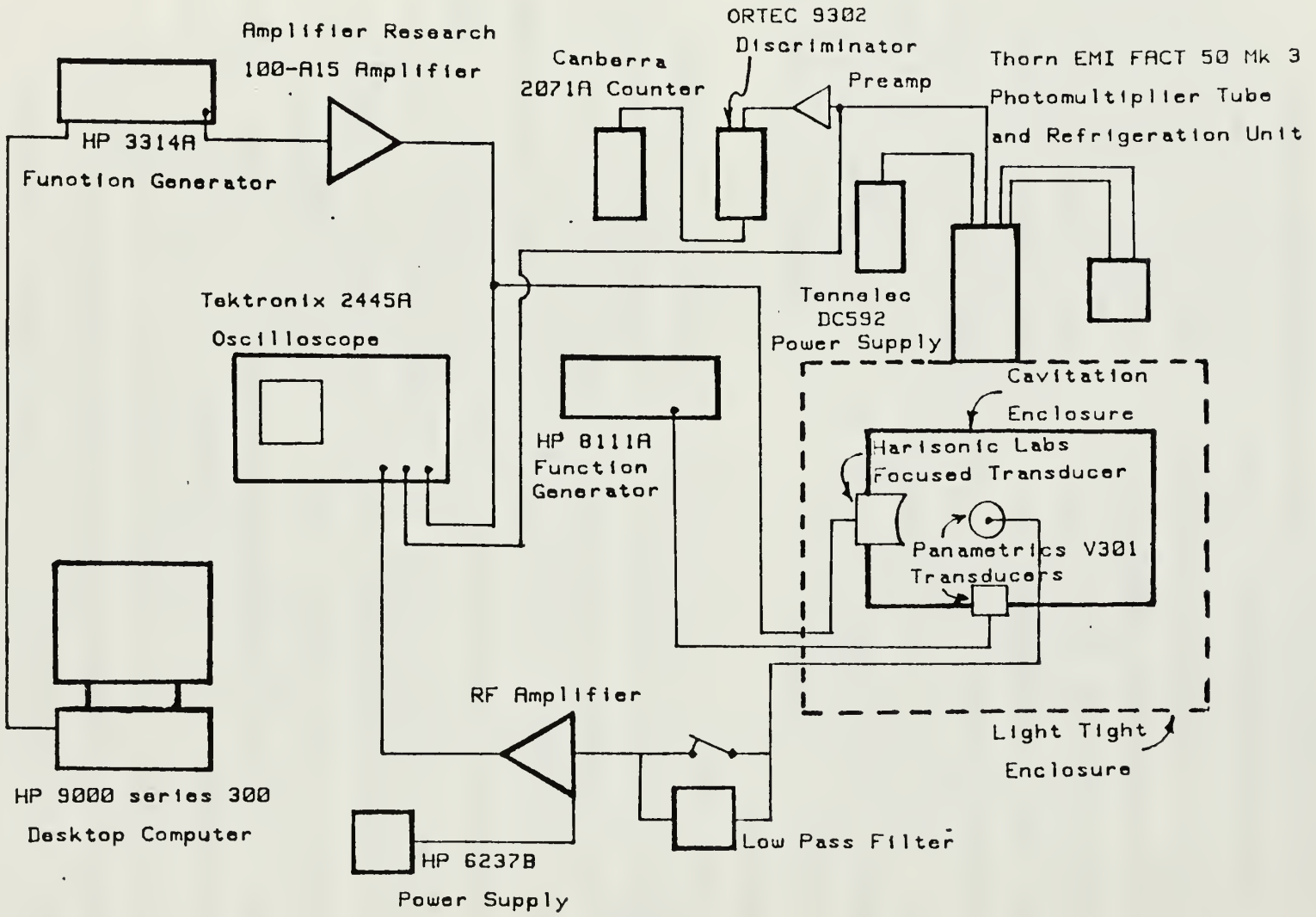

Figure 3.4

Cavitation Generation and Detection System

system operator must monitor the signal in the vicinity of this time delay for a transient that would indicate an increase in the scattered source signal, thus signifying the occurrence of a cavitation event. The operator must then manually interrupt the computer ramp function for the computer to calculate and display the threshold pressure.

In the active mode, the second Panametrics transducer is driven at a continuous frequency in the 100 kHz-500 kHz range. The resulting active signal is received by the detection transducer along with the source signal. The output of the detection transducer is passed through a low pass filter to remove the cavitation generation signal while passing the active detection signal. A sharp increase in the amplitude of the received signal indicates scattering from the bubble cloud that is formed by a cavitation event. The photomultiplier assembly and associated circuitry provide optical detection of the sonoluminescence generated by a transient cavitation event. The pulse from the PMT is pre-amplified and sent to an ORTEC 9302 pulse height discriminator, which determines the sensitivity of the mechanism. The discriminated signal is then sent through a Canberra 2071A counter. Because of background light noise within the light-tight enclosure, there is always some pulsed output from the PMT. Since transient events nearly always occur in groups, events will likely produce numbers of pulses significantly higher than background. At the time of this writing, attempts to detect cavitation via this method have proved unsuccessful.

E. TRANSDUCER CALIBRATION APPARATUS

In addition to the apparatus used for the generation and detection of cavitation, the apparatus used for the source transducer calibration is sufficiently involved to warrant further description. Calibration involves measuring the transverse and axial beam pattern of the source transducer and determining the transducer's total acoustic power output by force target deflection.

The axial and transverse beam patterns of both the source and detection transducers were found using a small PVDF probe hydrophone designed and built specifically for this use. The construction and calibration of this hydrophone were accomplished to fulfill requirements for a final project in a transducer theory and design course. Pertinent portions of the report submitted on the project are contained on Appendix B. The PVDF hydrophone was mounted in a micrometer jig that allowed precise measurement of its position relative to the transducer face (Figure 3.5).

The force target deflection measurement was used to determine peak output frequencies and total acoustic power output of the source transducers (Figure 3.6). A description of the theory behind the force target procedure follows in Chapter IV. In this procedure, the source transducer is driven by the function generator via the power amplifier at the same gain setting as will be used in the threshold experiment. The target is a small plexiglass plate, suspended at a 45-degree angle by four pieces of two-pound test monofilament fishing line of equal length (approximately .04 mm diameter, 225 μgrams/cm linear

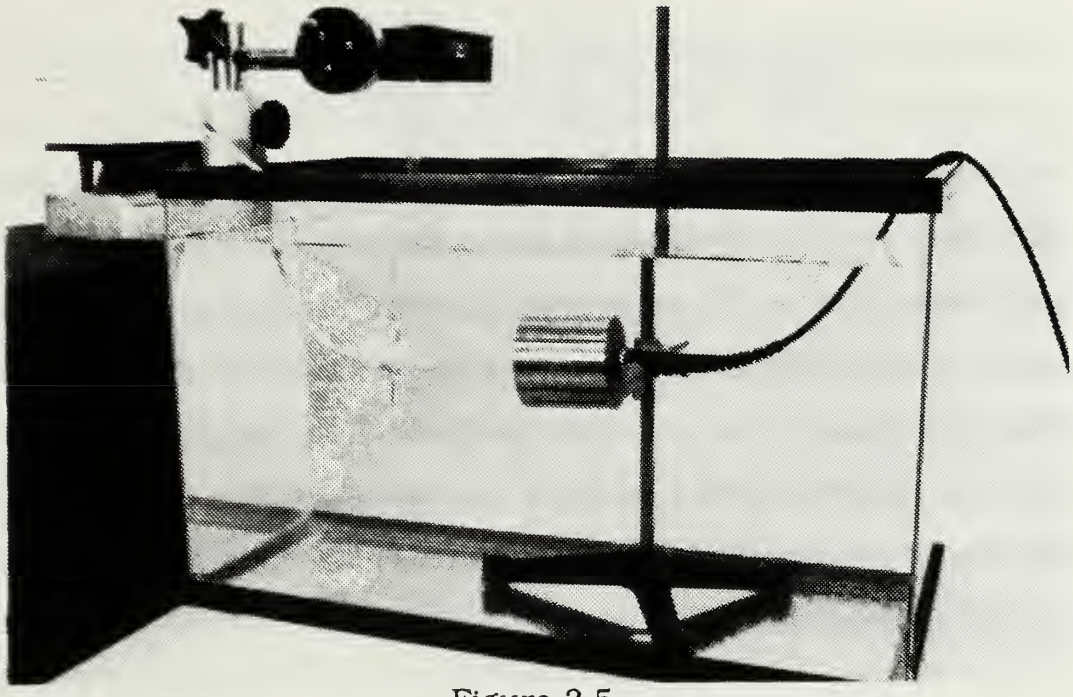

Figure 3.5

PVDF Hydrophone Determination of Source Transducer Beam Pattern

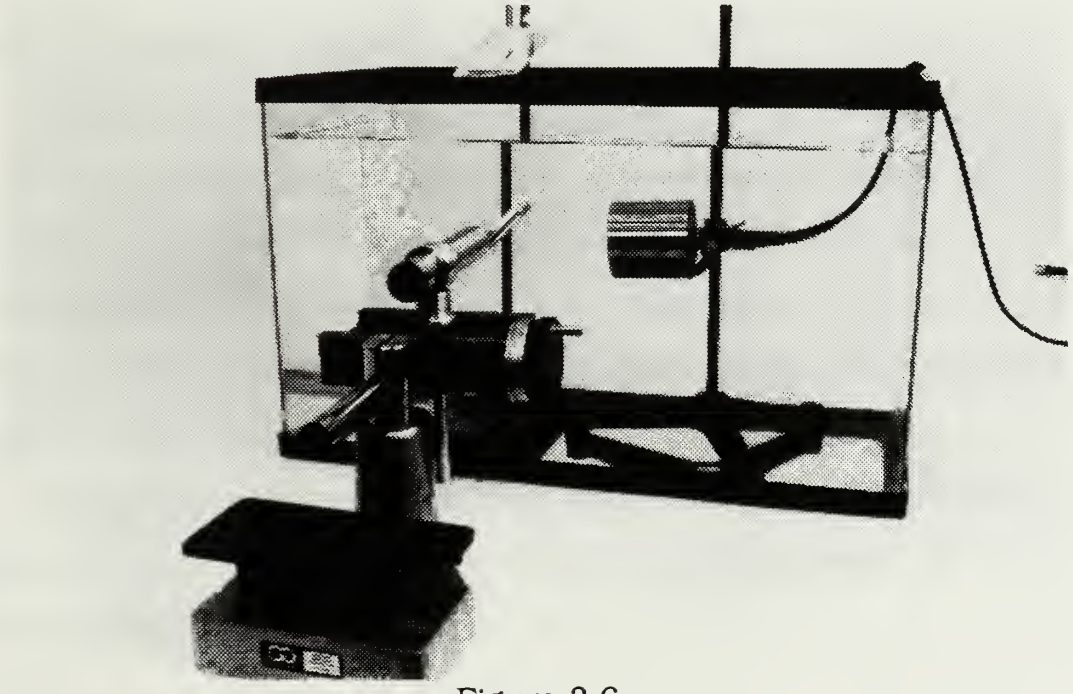

Figure 3.6

Equipment Arrangement for Force Target Deflection Measurements

density). The plexiglass target is rectangular in shape, of dimensions 3.8 x 5.1 x 0.7 cm. It has been carefully weighted using lead strips to achieve a weight of 1 g in water (14.7 g in air). A cavity approximately 0.3 cm deep is machined into the target and covered by a clear, thin, stiff plastic to form a pressure-release surface. This ensures that the radiation force is almost entirely transformed into a deflecting force. Essentially no acoustic energy is reflected back to the driving transducer, but rather toward the bottom of the test tank. The deflection was measured by a graduated telescope mounted to the micrometer jig described above.

IV. EXPERIMENTAL PROCEDURE

A. BACKGROUND

Prior to data taking, it is necessary to determine the performance characteristics of the transducers involved. This involves reciprocity calibration of the two Panametrics V301 transducers used for the acoustic detection of cavitation events. Also, once the source transducers' true peak output frequencies are determined, it is necessary to determine their axial and transverse beam patterns. These transducers are used to generate the ultrasonic field that induces cavitation. The axial beam patterns are used to verify the transducers' focal lengths while the transverse beam patterns are integrated to yield the effective area, A_{eff}, which relates peak intensity and total transducer output power.

Having determined the beam patterns, it is necessary to perform a radiation force-target deflection measurement of the Harisonic transducers in order to calculate transducer output power. Having experimentally determined A_{eff} and total power, the output peak intensity and consequently the output pressure characteristics can be accurately determined.

Upon completion of transducer source strength calibration, cavitation samples are prepared and threshold measurements are made in order to establish a data base.

B. RECIPROCITY CALIBRATION

The technique employed to find the sensitivities of the Panametrics V301 transducers is identical to that described in Reference 25. See Figure 4.1. The distance between transducers is 20.2 cm. This distance is well into the far field of the transmitter, which is found using the following approximation:

$$\frac{r_{min}}{L} \sim \frac{1}{4}\frac{L}{\lambda} \tag{4.1}$$

where

λ = acoustic wavelength 1.5 mm (assuming c = 1481 m/s for fresh water and f = 986 kHz),

L = diameter of V301 transducer = 3.2 cm,

r_{min} = minimum distance to the acoustic far field (in cm).

By employing the appropriate equations established in Reference 25, graphs of the transducers' sensitivities can be constructed. See Figure 4.2. The V301 transducers with serial numbers 596 and 598 were used.

C. AXIAL BEAM PATTERN MEASUREMENT OF SOURCE TRANSDUCERS

Using the polyvinylidene fluoride (PVDF) hydrophone discussed above (see Appendix B) and a precision measuring jig (see Figure 3.5), the axial beam patterns of the two Harisonic source transducers are determined. A CW sinusoid at the transducer's rated operating

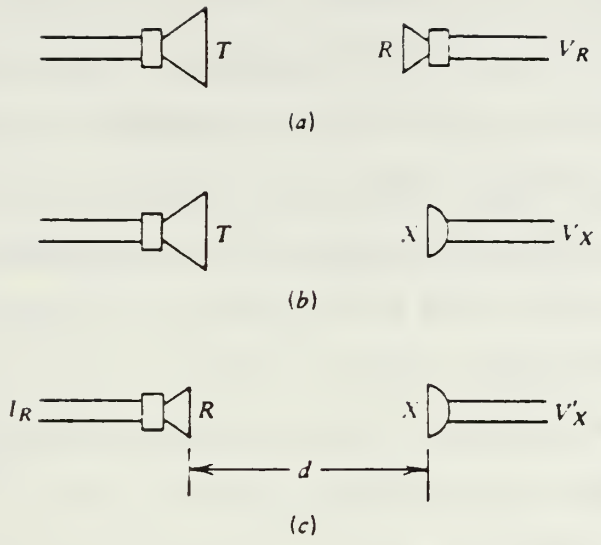

Figure 4.1

Reciprocity Calibration of Transducers (from [Ref. 25])

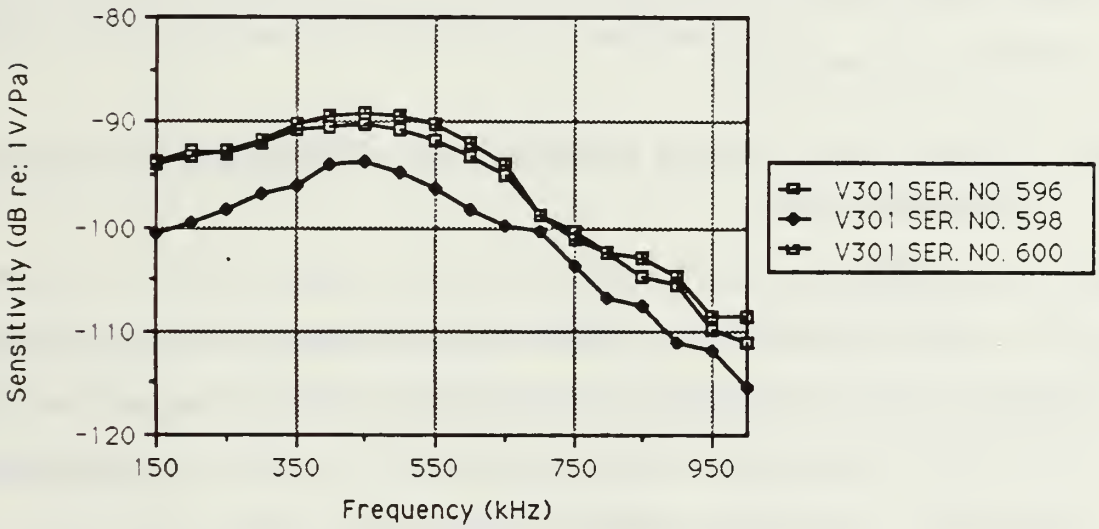

Figure 4.2

Sensitivity Calibration Results of 3 Panametrics V301 Transducers

frequency is generated by the HP 3314A function generator and passed through the Amplifier Research model 100A15 power amplifier and finally to the test transducer. The amplifier gain is set at 200 for a constant 15 VAC (peak-to-peak) output. The PVDF hydrophone is inserted into the mounting bracket attached to the measuring jig. The active element of the hydrophone is oriented such that the hydrophone face moves along the transducer's longitudinal axis as the micrometer knob is rotated. By recording the received voltage from the hydrophone and the position from the measuring jig's micrometer knob, an axial beam pattern can be determined and the transducer focal length verified. The Harisonic transducers used in this series of experiments were found to have focal lengths of 7.29 and 7.37 cm. There is not a large enough difference between these values and the rated focal length of 7.62 cm (3 in.) to warrant redesign of the cavitation tank or relocation of the transducers used for acoustic detection of cavitation.

D. TRANSVERSE BEAM PATTERN MEASUREMENT OF SOURCE TRANSDUCERS

1. Theory

It is necessary to relate peak intensity and total acoustic power in order to establish a relationship between transducer input voltage and transducer output pressure. In order to establish this relationship , we define an effective beam area A_{eff} by

$$A_{eff} = \frac{P_{TOT}}{I_{PEAK}}, \tag{4.2}$$

where I_{PEAK} = peak intensity (W/m^2) and P_{TOT} = total output power (W). Since $I \alpha p^2 \alpha V^2$, $I = K'V^2$ where K' is a constant; p is acoustic pressure and V is the corresponding hydrophone ouput voltage. This voltage, a function of distance from the center of the transducer face, is determined by a transverse scan of the focal region. At the focal point, $I_{PEAK} = K'V^2_{PEAK}$. Substituting this expression into equation (4.2) gives

$$A_{eff} = \frac{P_{TOT}}{K'V^2_{PEAK}}. \tag{4.3}$$

It is known that

$P_{TOT} = \int IdS$; dS = incremental area normal to the beam.

The integral is taken over the entire cross-sectional area of the beam and can be approximated (in polar coordinates) by

$$P_{TOT} \equiv \int_0^a \int_0^{2\pi} K'V^2 r dr d\theta = 2\pi K' \int_0^a V^2 r dr \tag{4.4}$$

where r = radial distance from transducer axis and a is some radial distance within which is contained practically all of the beam energy. In practice, a is chosen equal to the radius of the transducer face. Therefore,

$$A_{eff} = \frac{2\pi K' \int_0^a V^2 r dr}{K'V^2_{PEAK}} = \frac{2\pi \int_0^a V^2 r dr}{V^2_{PEAK}}. \tag{4.5}$$

Finally, since A_{eff} can be determined from the transverse beam profile, it is necessary only to calculate P_{TOT} (as described in a subsequent section) in order to calculate the peak intensity since $I_{PEAK} = P_{TOT}/A_{eff}$.

Further, since peak pressure, p_{PEAK}, is related to peak intensity by the following relationship (assuming either plane or spherical waves),

$$p_{PEAK} = (\rho_0 c I_{PEAK})^{1/2}, \tag{4.6}$$

p_{PEAK} can be rewritten in terms of A_{eff} and P_{TOT}:

$$p_{PEAK} = \left(\frac{\rho_0 c}{A_{eff}} P_{TOT}\right)^{1/2}. \tag{4.7}$$

2. Procedure

The procedure used for measuring transverse beam patterns is very similar to that described in the previous section. The jig is positioned in a manner such that the hydrophone travels in a line perpendicular to the longitudinal axis at a distance from the transducer face equal to the focal length. Accurate position measurements (±10 μm) can be made by recording the micrometer knob readings. Concurrently, hydrophone output voltages are recorded from the oscilloscope display, resulting in the transverse beam patterns of Figures 4.3 and 4.4. Plots of V^2r vs. r are included as Figures 4.5 and 4.6. Only the right half of each beam pattern was used to

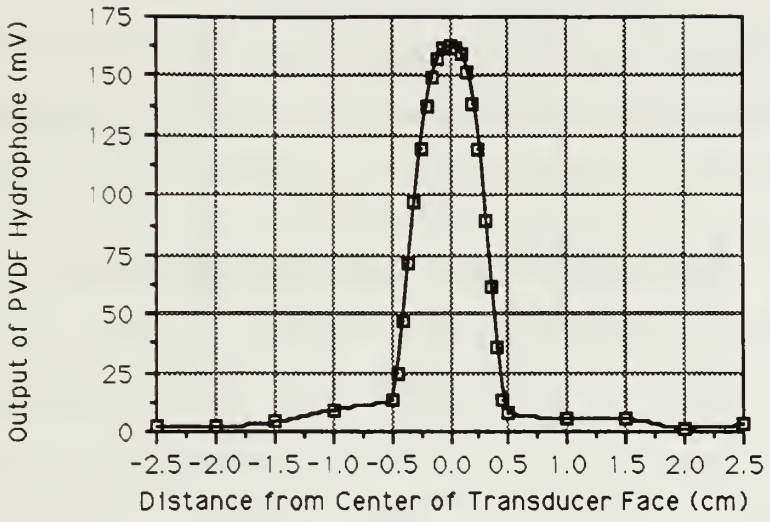

Figure 4.3

Transverse Beam Pattern of 1.0 MHz Transducer

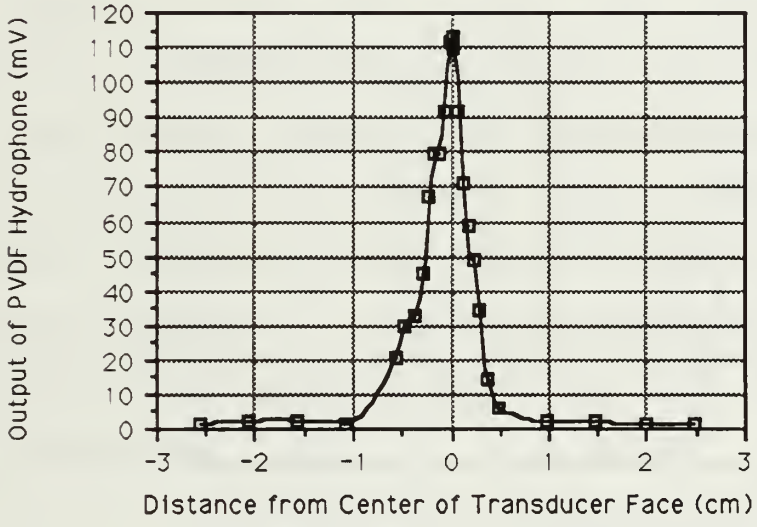

Figure 4.4

Transverse Beam Pattern of 2.25 MHz Source Transducer

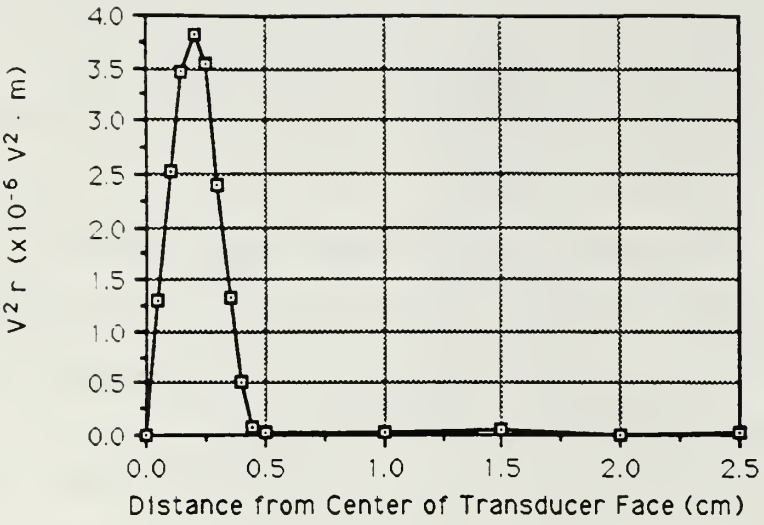

Figure 4.5

V^2r vs. r (Integrand of Equation (4.4)); 1.0 MHz Source Transducer

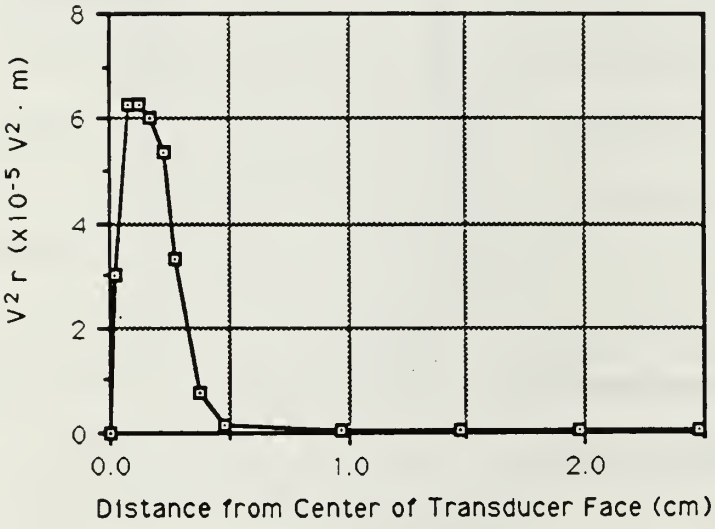

Figure 4.6

V^2r vs. r (Integrand of Equation (4.4)); 2.25 MHz Source Transducer

be symmetrical. This is not exactly true, but no appreciable error is introduced by making this assumption. Integrations of these plots are performed by using a Macintosh Plus personal computer and DBGPLOT software. The results are plotted in Figures 4.7 and 4.8.

E. DETERMINATION OF TRANSDUCER PEAK OUTPUT FREQUENCY

In order to optimize the output from the source transducers, it is necessary to know their peak output frequency. Using the deflection apparatus illustrated in Figure 3.6, the rectangular target is suspended in the focal region of a source transducer. A sinusoidal signal at the rated operating frequency is applied to the transducer via the power amplifier. A constant input voltage of 15 volts (peak to peak) is maintained (monitored on the oscilloscope) while frequency is varied above and below the manufacturer's quoted peak output values. Target deflection is measured for the various test input frequencies by noting the change in target position with a graduated telescope mounted on the measuring jig used previously. Plots of target deflection versus transducer frequency are reproduced as Figures 4.9 and 4.10. The transducers specified as 1 MHz and 2.25 MHz peak output frequencies were found to have true peak output frequencies of 986 kHz and 2.17 MHz, respectively.

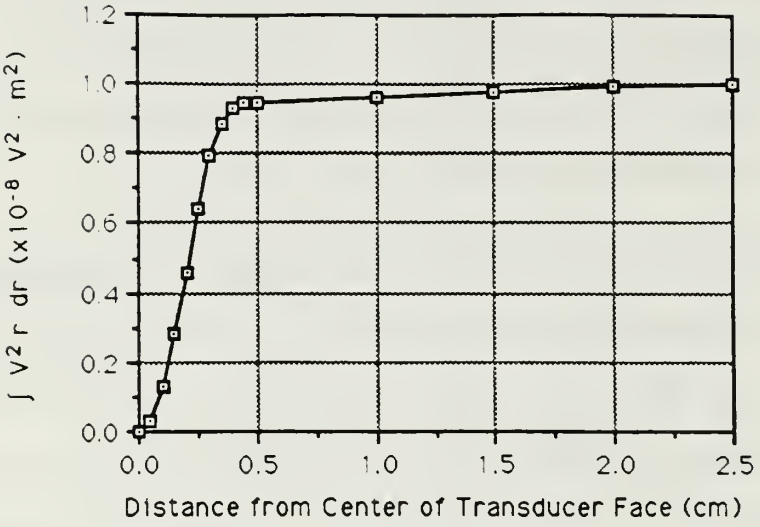

Figure 4.7

Integral of V^2rdr for 1.0 MHz Transducer

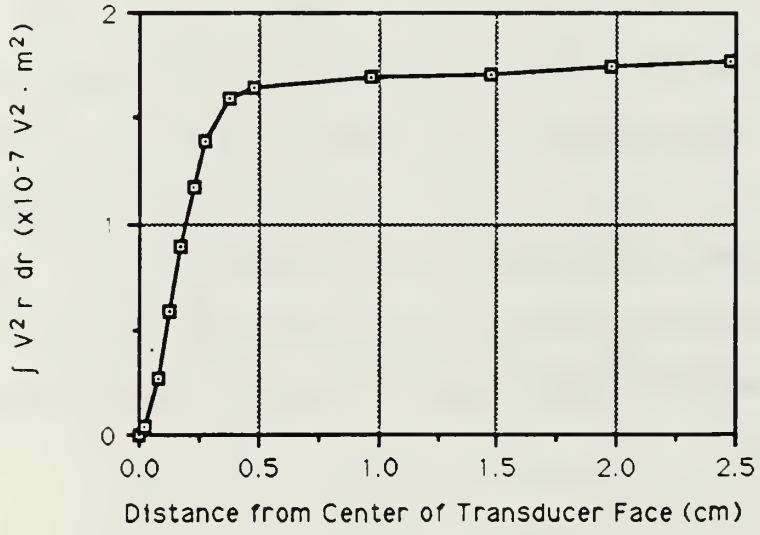

Figure 4.8

Integral of V^2rdr for 2.25 MHz Transducer

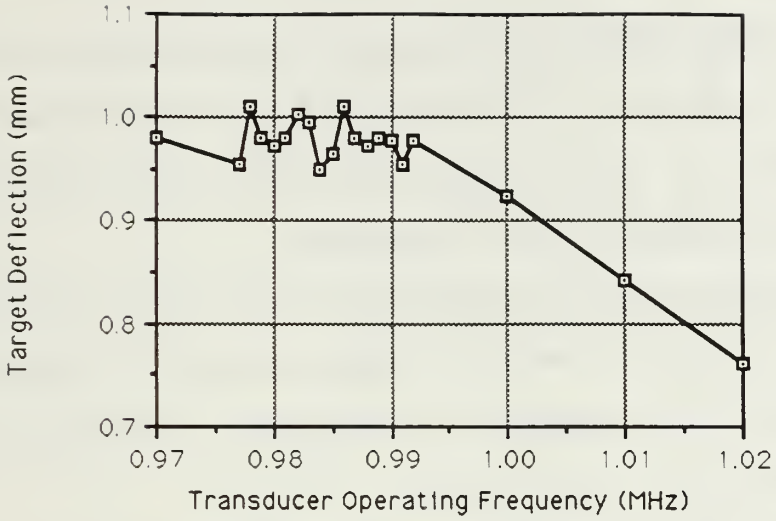

Figure 4.9

Target Deflection versus Frequency for Determination of Peak Operating Frequency of 1.0 MHz Source Transducer

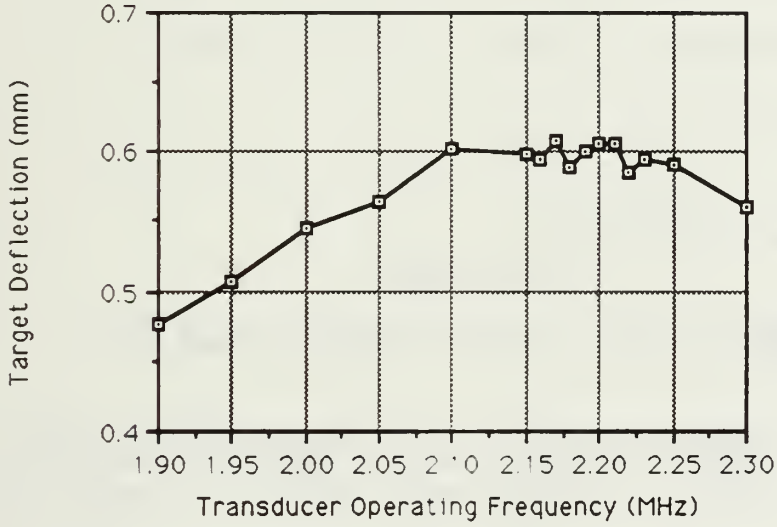

Figure 4.10

Target Deflection versus Frequency for Determination of Peak Operating Frequency of 2.25 MHz Source Transducer

F. RADIATION FORCE–TARGET DEFLECTION MEASUREMENT

1. Theory

The method used to determine the peak output pressure of the Harisonic transducers is a variation of the method described by Dunn, et al. [Ref. 26]. Rather than using a sphere, as in Dunn's work, the rectangular plexiglass target is employed.

A rectangular target is used rather than a sphere because, as a sphere deflects, it tends to move out of the sound field, while a relatively large plate is less susceptible to this effect. In addition, there is no need to calculate the form function.

Referring to Figure 4.11 (reproduced from Reference 26 with some clarifying remarks), it is a relatively simple matter to construct the appropriate free-body diagram and the equations governing the static equilibrium:

$$\Sigma F_x = -F_r + T\cos\theta = 0,$$

$$\Sigma F_y = -mg + T\sin\theta = 0.$$

The above equations imply that

$$T = \frac{F_r}{\cos\theta} = \frac{mg}{\sin\theta}. \tag{4.8}$$

Therefore, $F_r = \frac{mg}{\tan\theta}$. However, $\tan\theta = \frac{L-h}{d}$. If $L \gg h$, $\tan\theta \approx L/d$. Therefore,

$$F_r = \frac{mg}{\tan\theta} \cong \frac{mg}{\left(\frac{L}{d}\right)} = \frac{mgd}{L}. \tag{4.9}$$

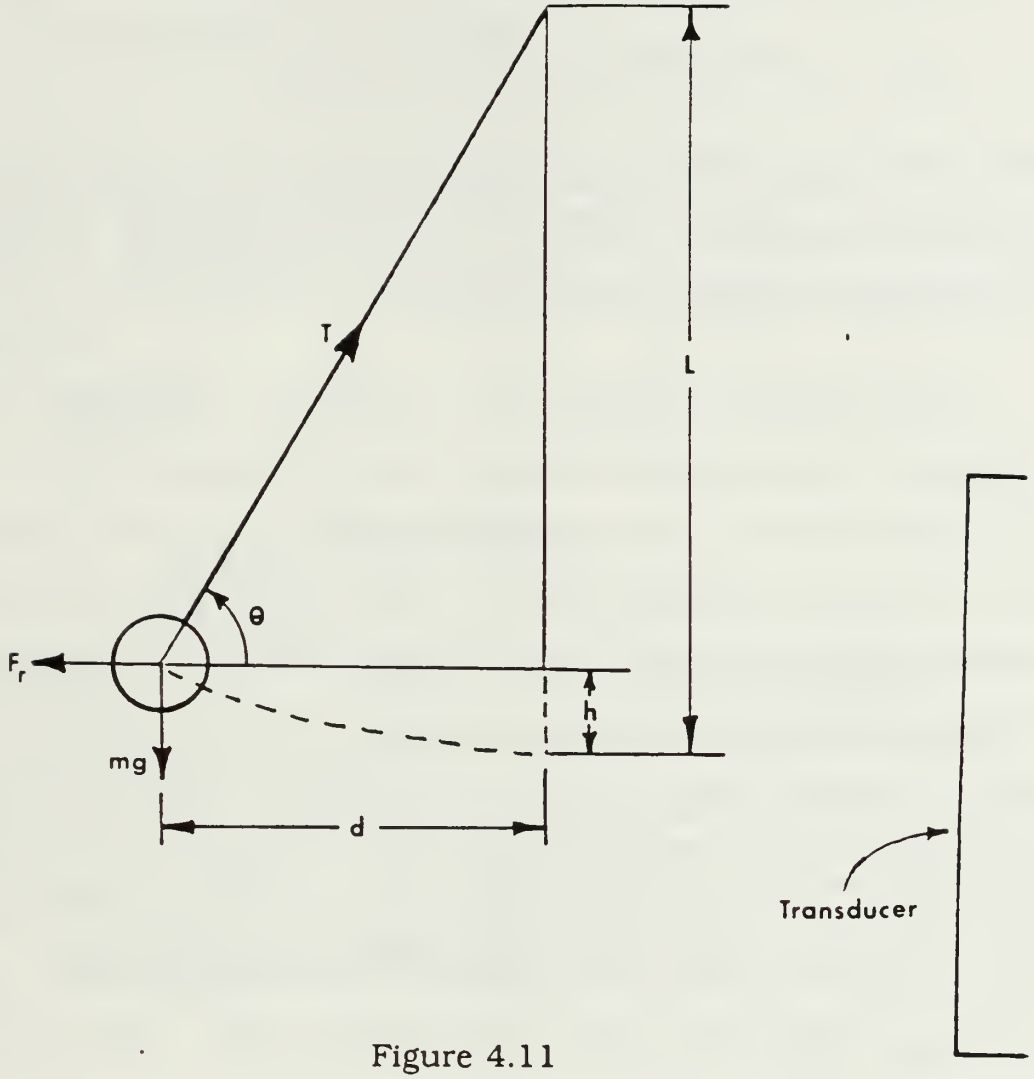

Figure 4.11

Free Body Diagram of Force Target Deflection

From References 25 and 27, it can be shown that the excess pressure $p_e = \rho c^2 s$, where ρ = density of the medium, s = condensation, and c = phase speed of the acoustic waves. For a high-intensity sound field, variations in density are significant, so $\rho \cong \rho_0(1 + s)$. By substitution,

$p_e = \rho c^2 s \cong \rho_0(1 + s)c^2 s = \rho_0 c^2 s + \rho_0 c^2 s^2$. If $s = s_0 \cos\omega t$, the time-averaged excess pressure, $\langle p_e \rangle_t$, can be rewritten as follows:

$$\langle p_e \rangle_t = \rho_0 c^2 s_0 \langle \cos\omega t \rangle + \rho_0 c^2 s_0^2 \langle \cos^2 \omega t \rangle.$$

The first term on the right-hand side reduces to zero, but the second term (or radiation pressure) can be expanded by employing the appropriate trigonometric identity.

$$\rho_0 c^2 s_0^2 \langle \cos^2 \omega t \rangle = \rho_0 c^2 s_0^2 \cdot \frac{1}{2} [1 + \langle \cos^2 \omega t \rangle]$$

$$= \frac{\rho_0 c^2 s_0^2}{2} + \frac{\rho_0 c^2 s_0^2}{2} \langle \cos 2\omega t \rangle.$$

This reduces finally to $\rho_0 c^2 s_0^2 \langle \cos^2 \omega t \rangle = \frac{\rho_0 c^2 s_0^2}{2}$. However, $p_e = \frac{I}{c}$ where I = intensity. Recalling that power, $P_{TOT} = I \cdot A$ where A = area, it can be seen that the relationship $P_{TOT} = \langle p_e \rangle_t cA$ is also true. Setting $\langle p_e \rangle_t \cdot A = F_r$, $P_{TOT} = \frac{F_r}{A} cA = F_r \cdot c$ where c = 1481 m/s since these tests are conducted in fresh water. By substitution,

$$P_{TOT} = \frac{mgc}{L} \cdot d \qquad (4.10)$$

where $\frac{mgc}{L}$ is a constant and d is the measured target deflection.

By substituting the appropriate values for m, g, c, and L,

$$P_{TOT} = \frac{(0.99 \times 10^{-3}\ kg)\ (9.8\ m/s^2)\ (1481\ m/s)}{14.05 \times 10^{-2}\ m} \cdot d;$$

$$= \left(1.02 \times 10^2 \frac{N}{s}\right) \cdot d;\ d \text{ in meters.}$$

This equation is used in the radiation force-target deflection measurements. Upon completion of such measurements, all ingredients necessary to characterize transducer output pressure will have been determined.

2. Procedure

A CW sinusoid (at the transducer's peak output frequency) generated by the HP 3314A function generator is sent through the Amplifier Research model 100A15 power amplifier and finally to the Harisonic transducer undergoing test. The deflection of the plexiglass target is measured as the transducer input voltage (as monitored on the Tektronix 2445A oscilloscope) is varied. Plots of target deflection vs. input voltage squared are included as Figures 4.12 and 4.13. The slopes of these plots are proportional to output power for a given input voltage. Note that the "mirror" images of the recorded data points are plotted as well. This ensures that a line determined by linear regression will pass through the origin, resulting in zero power output for zero input voltage, as is dictated by common sense.

Having determined all of the terms necessary to characterize output pressure, the pressure as a function of input voltage can be plotted. See Figures 4.14 and 4.15. Again, the "mirror" images are plotted as well in order to drive the linear regression through the

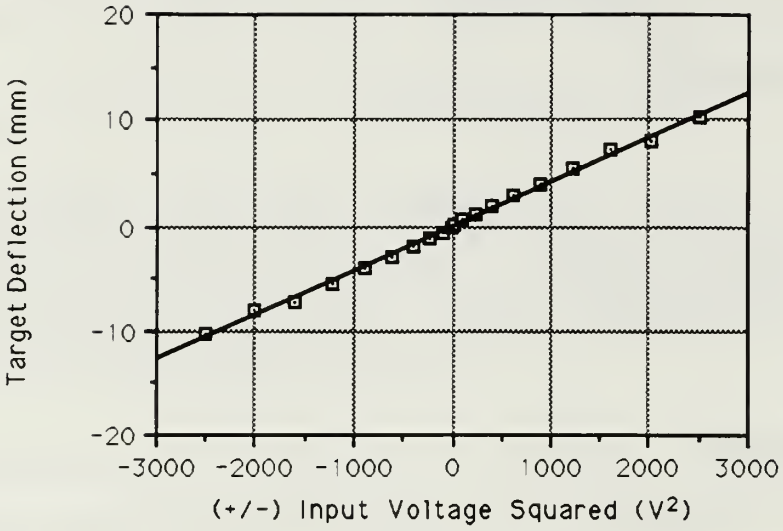

Figure 4.12

Target Deflection vs. V^2 for Source Transducer Calibration 1.0 MHz

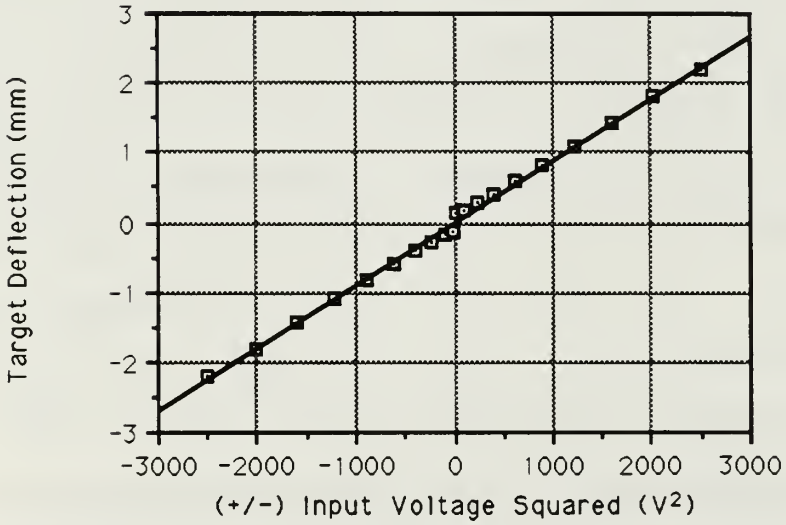

Figure 4.13

Target Deflection vs. V^2 for Source Transducer Calibration 2.25 MHz

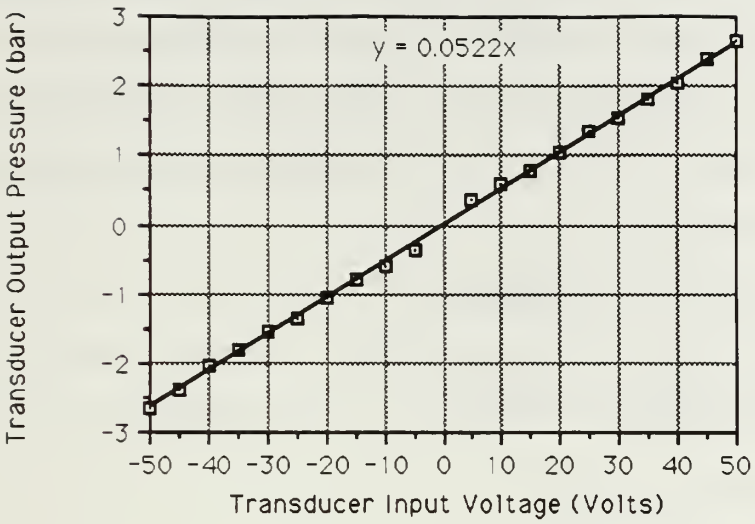

Figure 4.14

Output Pressure Amplitude vs. Input Voltage for 1.0 MHz Source Transducer

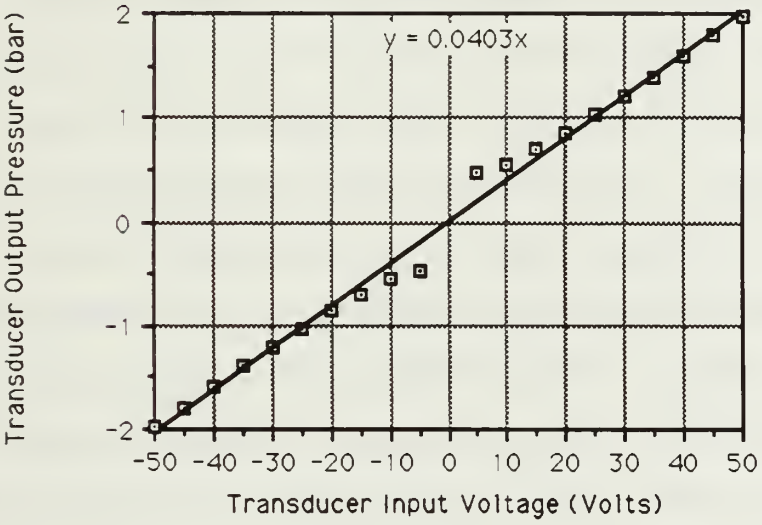

Figure 4.15

Output Pressure Amplitude vs. Input Voltage for 2.25 MHz Source Transducer

origin. Note that, in Figure 4.15, the relatively large deviations from the linear regression at lower voltages are of no concern since the transducer is not operated in this region. The relationships between the peak-to-peak transducer input voltage and the peak output pressure are included below.

For the 1 MHz transducer:

$$p_{PEAK}\ (\text{bar}) = 0.0522\ V_{IN}\ (\text{mV}).$$

For the 2.25 MHz transducer:

$$p_{PEAK}\ (\text{bar}) = 0.0403\ V_{IN}\ (\text{mV}).$$

G. DETERMINATION OF TRANSIENT CAVITATION THRESHOLDS

All threshold data were taken using the passive acoustic (scattering of the source signal from the bubble "cloud" produced by a transient event) detection scheme. This method was the first to show acceptable reliability. As the data required was substantial and exceptionally time-consuming to take, we concentrated on data accumulation via this method rather than sacrifice more time refining the other two detection methods. The HP 9000 series 300 computer was programmed to allow user input of desired frequency, pulse repetition frequency (PRF), pulse duration, and pressure amplitude sweep parameters (via input of function generator starting amplitude, voltage amplitude increase per step, and total number of amplitude steps). Data was obtained at 986 kHz and 2.17 MHz using 200 Hz, 500 Hz,

and 1000 Hz PRF. Pulse durations of 1.5, 2, 5, 10, 15, 20, 25, 30, 35, and 40 μsec were examined. All voltage ramps were started at 300–400 mV peak input voltage to the power amplifier, which results in an initial peak output pressure from the source transducers of approximately 3–4 bar. Incrementally increasing pressure steps of .1 bar were held for 1.5 seconds. The ramps were continued until a cavitation event was detected. Twenty threshold measurements were taken at each pulse duration, PRF, and frequency combination.

V. RESULTS, DISCUSSION, RECOMMENDATIONS

A. RESULTS AND DISCUSSION

Figures 5.1 and 5.2 are graphs of threshold pressure versus pulse duration taken at 986 kHz with PRFs of 200 Hz and 1000 Hz, respectively. The error bars in these and subsequent figures represent one standard deviation of the data above and one standard deviation below the mean threshold pressure. It should be noted that thresholds were undetectable at the 2 μsec pulse width for the 200 Hz PRF, most likely due to lack of scattered signal from a two-cycle burst at such a low PRF. At 1000 Hz PRF, the thresholds are essentially constant down to the 10 μsec pulse duration. At 5 and 2 μsec pulse durations, the thresholds show a marked increase. The data in Figures 5.1 and 5.2 show good agreement with Reference 6.

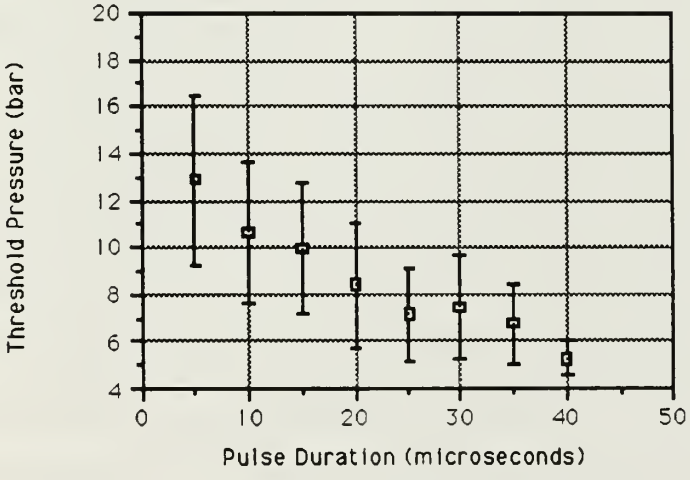

Figure 5.1

Threshold Pressure vs. Pulse Duration 986 kHz, 200 Hz PRF

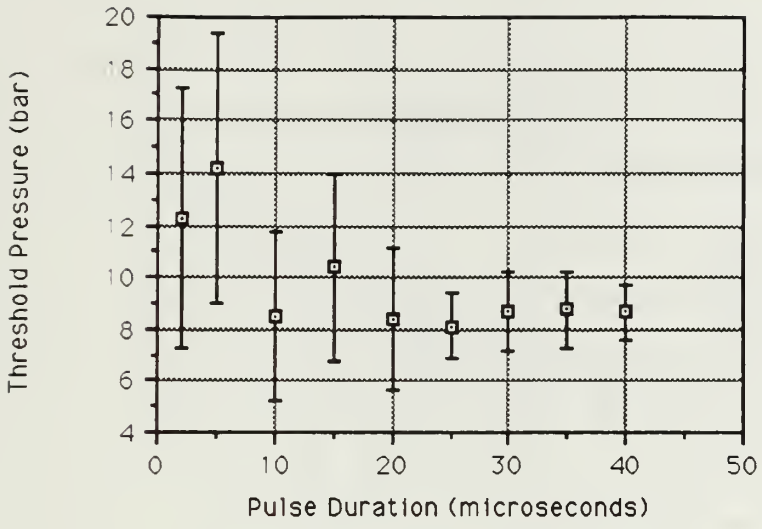

Figure 5.2

Threshold Pressure vs. Pulse Duration 986 kHz, 1000 Hz PRF

Figures 5.3 and 5.4 are graphs of threshold pressure versus pulse duration at 2.17 MHz for PRFs of 200 and 1000 Hz, respectively. There is an essentially constant threshold at 200 Hz PRF for pulse durations of 15 μsec and larger, while shorter pulse durations indicate a marked increase in threshold pressure. In contrast, however, at 1000 Hz PRF, the thresholds are essentially constant for all pulse durations down to 2 μsec, with a marked increase evident at a pulse duration of 1.5 μsec.

Figure 5.5 is a comparison of the thresholds obtained for the two source frequencies at 200 Hz PRF; Figure 5.6 is the same at 1000 Hz PRF. These results support theoretical predictions by Flynn [Ref. 4] and Apfel [Ref. 3] that the threshold is independent of frequency for sufficiently small cavitation nuclei. For parameters used in this

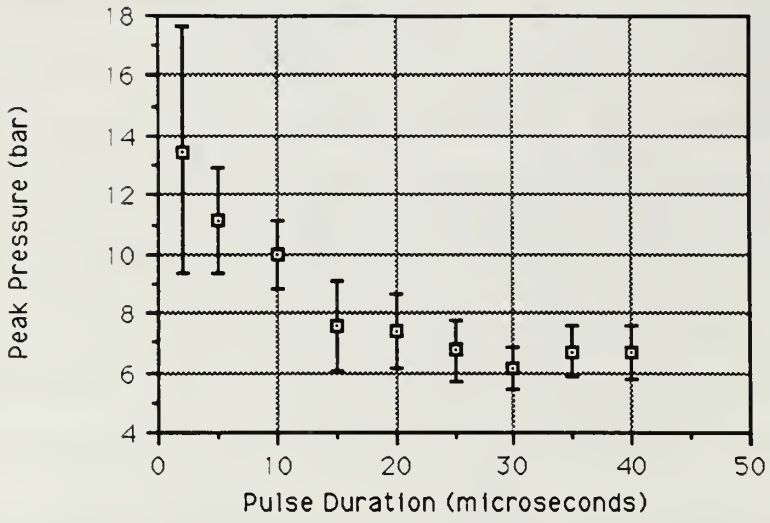

Figure 5.3

Threshold Pressure vs. Pulse Duration 2.17 MHz, 200 Hz PRF

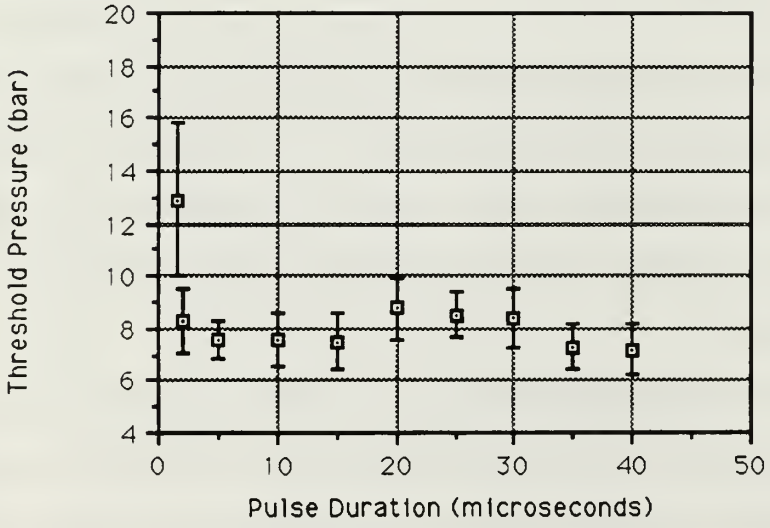

Figure 5.4

Threshold Pressure vs. Pulse Duration 2.17 MHz, 1000 Hz PRF

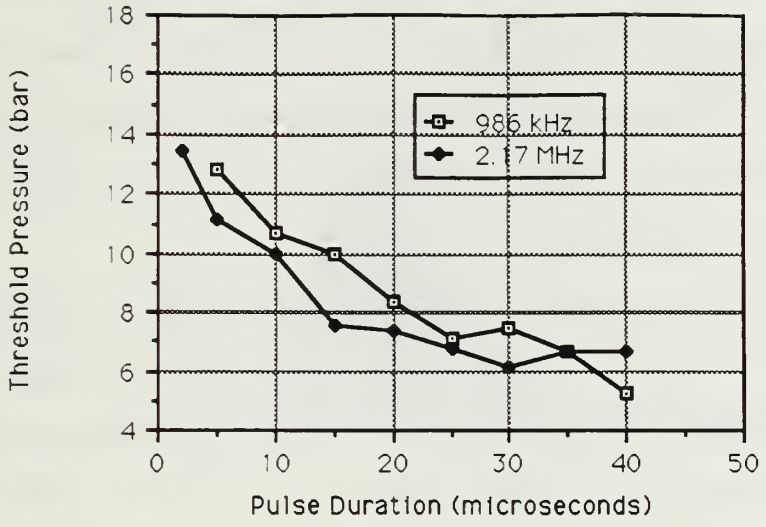

Figure 5.5

Threshold Pressure vs. Pulse Duration
986 kHz and 2.17 MHz at 200 Hz PRF

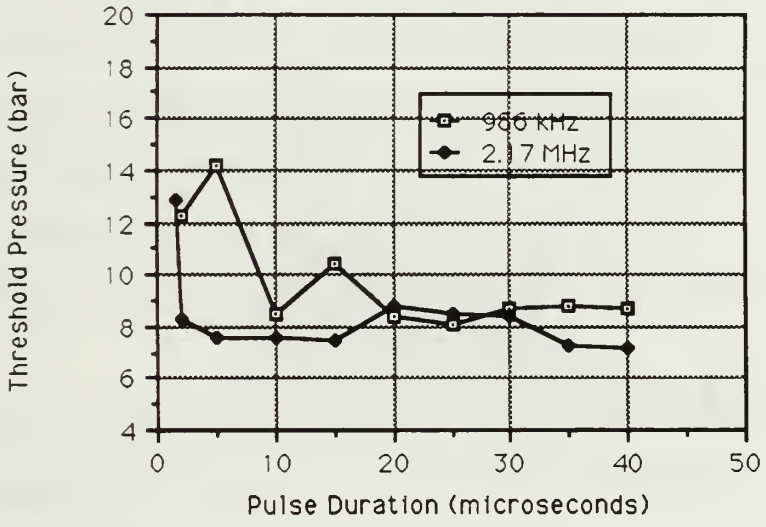

Figure 5.6

Threshold Pressure vs. Pulse Duration
986 kHz and 2.17 MHz at 1000 Hz PRF

experiment, threshold pressure values are essentially equal to Blake pressure thresholds, which have no frequency dependence (see equation 2.11). This conclusion is valud due to the close relationship between transient and Blake thresholds for the frequencies under consideration (see Figure 2.3).

Figure 5.7 is a histogram of pressure thresholds (rounded to the nearest bar) measured for each individual transient cavitation event. Again from equation (2.11) above, there is a direct relationship between bubble size and Blake threshold pressure. Figures 5.8 through 5.11 are histograms of threshold measurements for individual frequency/PRF combinations. It should be noted that the graphs may be slightly skewed due to the starting pressure amplitudes of most ramps. Since our experience indicated that expected threshold pressures were in the 6–9 bar range, source pressure ramps were started in the 3–4 bar range. An occasional low threshold event due to the presence of an unusually large nucleus may have been missed. Keeping this in mind, it appears that all histograms except Figure 5.8 exhibit a roughly Gaussian distribution with mean values in the 7–8 bar range. This corresponds to bubble radii in the range of 0.075–0.09 μm.

As stated above, when larger pulse width measurements are compared in Figures 5.5 and 5.6, the thresholds are independent of pulse duration. As pulse durations decrease, there is an increase in threshold. This observation would indicate that the larger pulse

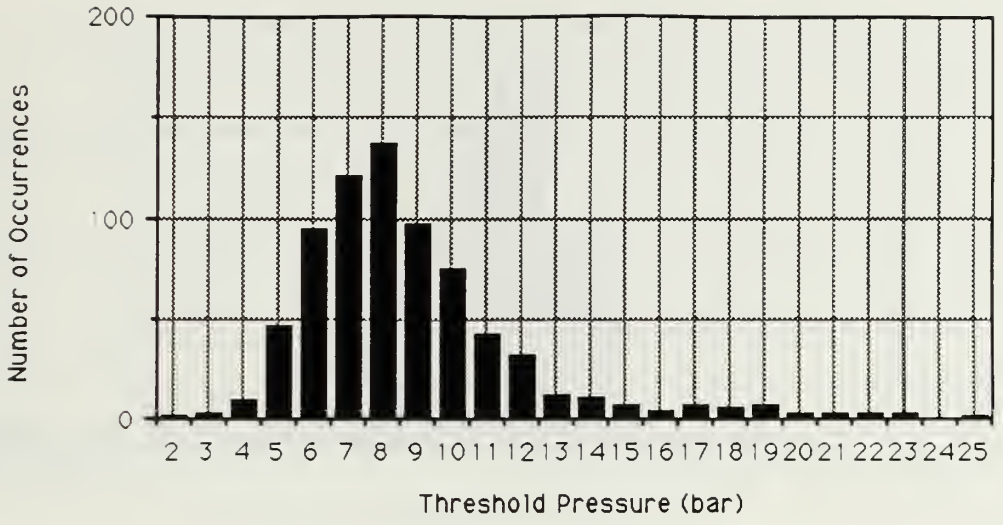

Figure 5.7

Histogram of All Threshold Pressure Measurements (rounded to nearest bar)

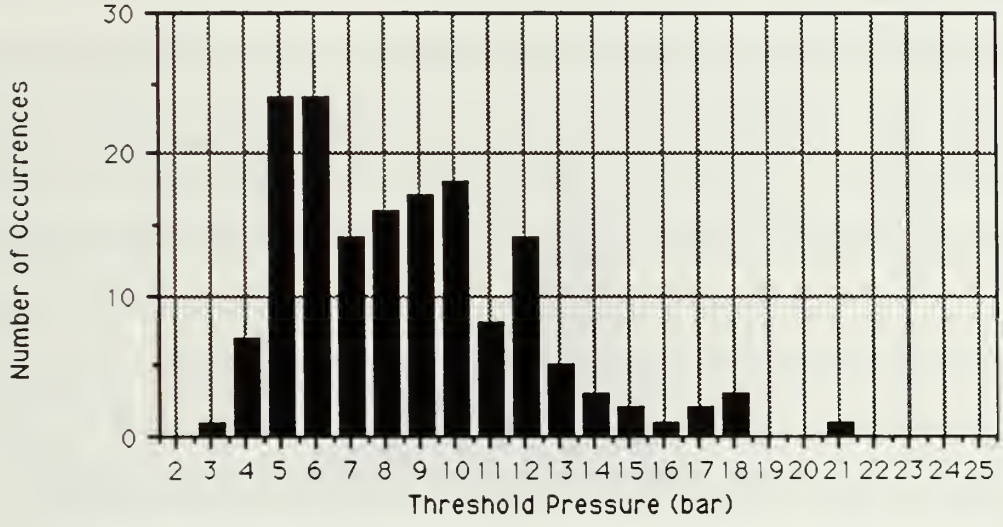

Figure 5.8

Histogram of All Threshold Pressure Measurements 986 kHz, 200 Hz PRF

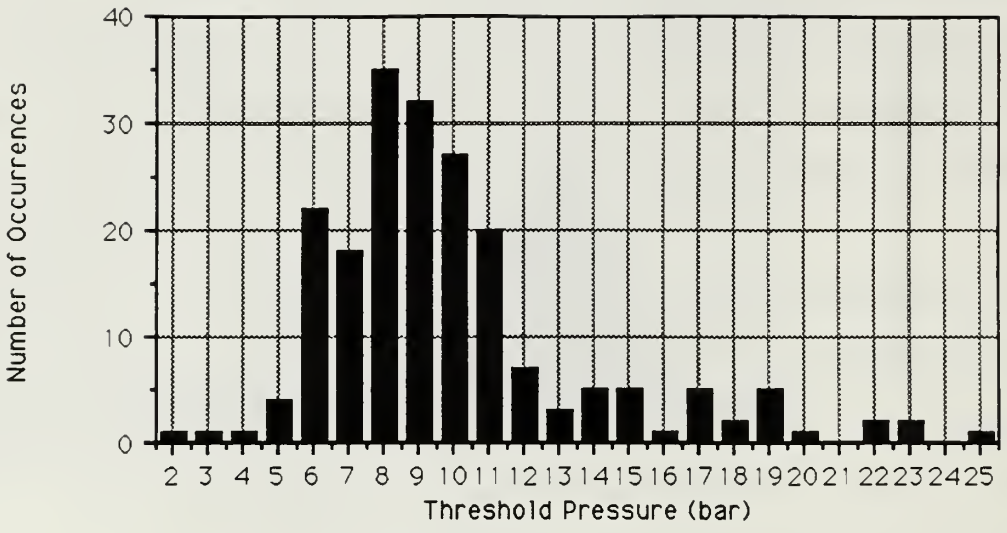

Figure 5.9

Histogram of All Threshold Pressure Measurements
986 kHz, 1000 Hz PRF

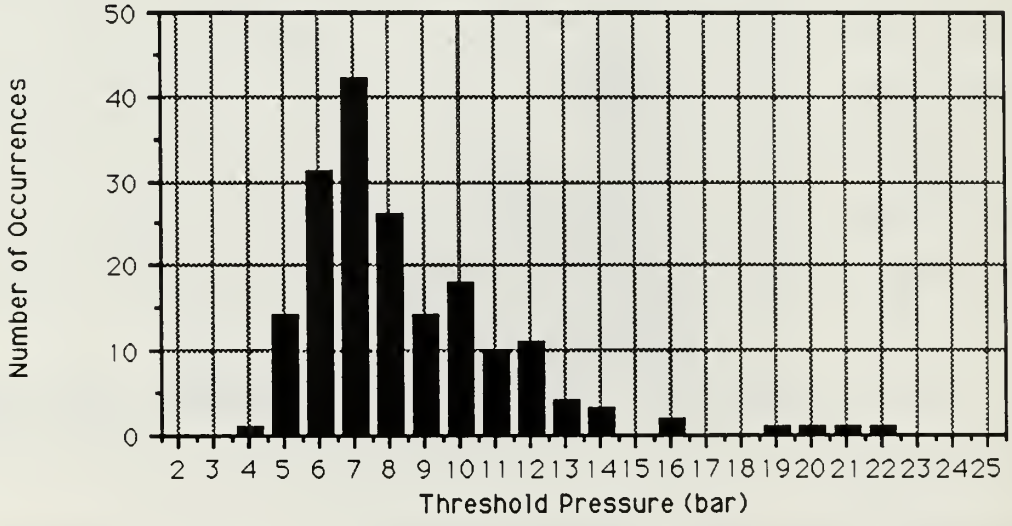

Figure 5.10

Histogram of All Threshold Pressure Measurements
2.17 MHz, 200 Hz PRF

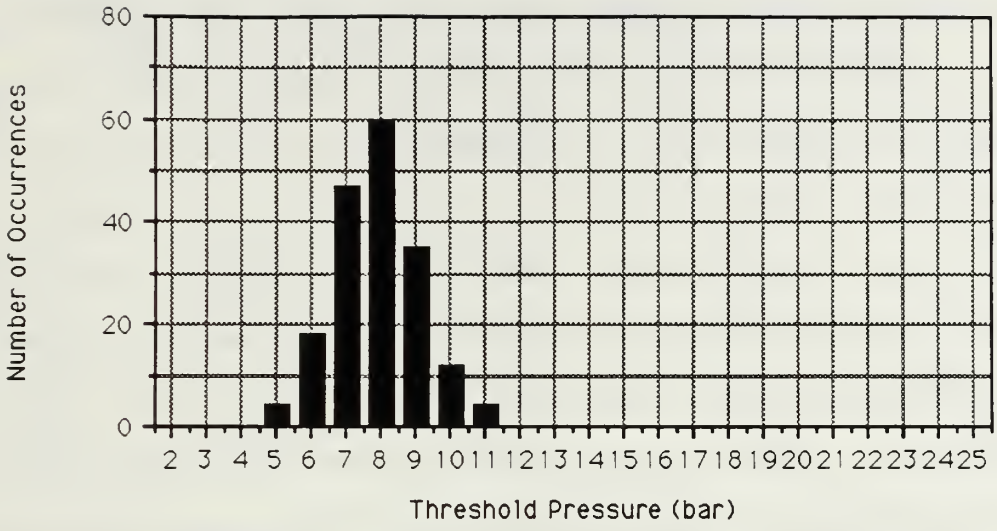

Figure 5.11

Histogram of All Threshold Pressure Measurements
2.17 MHz, 1000 Hz PRF

durations allow time for a growth mechanism, such as rectified diffusion, to cause nuclei to evolve to a Blake or transient threshold radius. There appears to be insufficient time for the growth mechanism to take effect at shorter pulse durations. It is postulated that, during the rest time between pulses, nuclei dissolve to their original equilibrium sizes.

Further examination of Figures 5.1 through 5.4 reveals that there is a distinct relationship between the flat and sloped portions of the graphs. Specifically, Figure 5.1 (low frequency/low PRF) reveals a continuously decreasing threshold pressure for increasing pulse duration. Although no additional data was taken at pulse durations greater than 40 μsec, there were essentially no thresholds recorded at

levels lower than the threshold determined at that point, so it is anticipated that the graph flattens out beyond this point. An attempt was made to evaluate this hypothesis experimentally, but problems were encountered with the 986 kHz source transducer that prevented any further reliable data from being obtained at that frequency. Figure 5.2 (low frequency/high PRF) shows relatively flat threshold measurements for pulse durations of 10 μsec and greater, with significantly higher thresholds occurring at 5 and 2 μsec pulse durations. Figure 5.3 (high frequency/low PRF) shows flat threshold measurements for pulse durations of 15–20 μsec and greater, and increasing thresholds for 10, 5, and 2 μsec pulse durations. Finally, Figure 5.4 (high frequency/high PRF) shows essentially flat threshold measurements down to 2 μsec pulse duration. This observation prompted an additional set of 10 threshold measurements at 2.17 MHz, 1000 Hz PRF, and 1.5 μsec pulse duration (3 cycles per pulse) to ascertain whether there was a rise in threshold below 2 μsec. The mean value of the ten readings was 12.9 bar, with standard deviation of 2.90, which indicates a "knee" in this graph as well in the vicinity of the 2 μsec pulse duration. There appears to be a relationship between frequency, pulse duration, and PRF which allows a certain range of pulses per unit time to mark the break point where shorter pulse durations begin to affect cavitation thresholds. In Reference 6 it was postulated that threshold became independent of pulse duration when pulses contained more than 10 cycles. Our measurements show the "knee" to be located as indicated in Table 5.1:

TABLE 5.1

CYCLES PER UNIT TIME FOR VARIOUS FREQUENCY, PRF, AND PULSE DURATION COMBINATIONS

f	PRF	Pulse length ("KNEE")	Cycles/pulse	Cycles/sec (PRF x Cycles/pulse)
986 kHz	200 Hz	40 μsec	40	8,000
986 kHz	1000 Hz	10 μsec	10	10,000
2.17 MHz	200 Hz	15 μsec	33	6,600
2.17 MHz	1000 Hz	2 μsec	4	4,000

Although the value of PRF x (cycles/pulse) product varies from 4,000 to 10,000, this analysis indicates that the knee of the graph is predictable within a reasonable range of pulse widths. In addition, our choice of pulse widths was not geared toward finding this break point of the graph. There may be other pulse durations that more accurately indicate the knee between those examined which yield a narrower range of cycles per unit time values. To test the hypothesis, a series of threshold measurements were taken at 2.17 MHz and 500 Hz PRF. It was anticipated that the knee of the curve should occur in the vicinity of the 10 μsec pulse duration. Figure 5.12, which illustrates the results of these measurements, shows that the knee occurs as predicted. Although it is not prudent to generalize when discussing mechanisms as complex as bubble dynamics in sound fields, it is felt that this aspect of these findings bears further investigation.

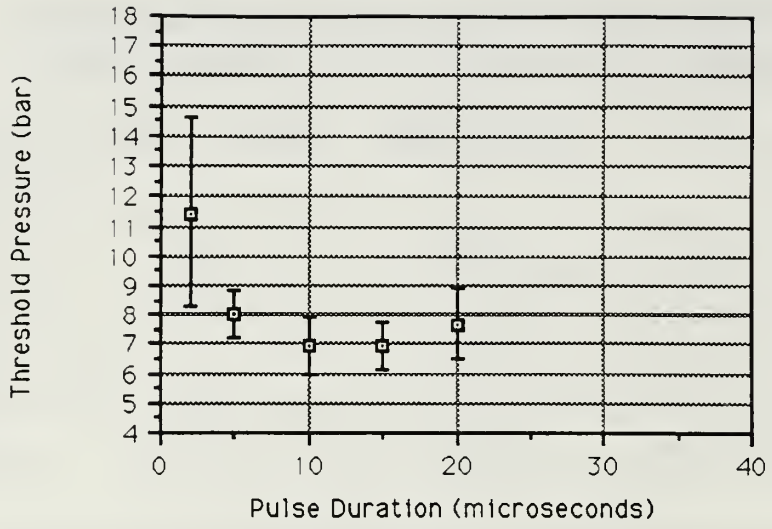

Figure 5-12

Threshold Pressure vs. Pulse Duration 2.17 MHz, 500 Hz PRF

B. RECOMMENDATIONS

All experimental measurements were taken using the passive acoustic scattering method, which proved to be an excellent detection method when pulse widths were large. The resulting signal scattered from the bubble "cloud" generated by the cavitation event resulted in a clear, distinct indication of a transient event. As pulse durations were decreased, however, the scattered signal was sometimes weak and lacking definition. It is essential that sonoluminescence detection and/or active acoustic detection schemes be fully incorporated into the procedures to minimize any systematic errors that may exist in the passive detection system. The optical detection system was limited only by unavailability of luminol (a sonoluminescence enhancer) until the very final weeks of the project. By then, it was too

late to bring the system to full operation. It is anticipated that this system, when fully operational, will allow the replacement of the human element of the current detection scheme with the electronics system. As gathering of cavitation data via manual observation of the transient signals on an oscilloscope requires exceptional vigilance and perseverance on the part of the operators, fully automating the detection mechanism is essential to the continued success of this apparatus.

It is recommended, when the system is fully operational, that additional threshold measurements be taken at specific pulse duration/PRF/frequency combinations in order to confirm the cycles per unit time effect noted in the hypothesis above. Extremely low or high PRFs (10 Hz, 8 kHz) should indicate whether the hypothesis has merit. Localization of a specific number of pulses or period of insonification which marks the knee of the threshold curve may lead to a better determination of the mechanisms which allow the cavitation events to fully evolve.

APPENDIX A

APPARATUS CONTROL PROGRAM "CAVDAT"

```
10    !*************************************************************************
20    !* PROGRAMMERS:  R.L. BRUCE AND R.D. MIDDLETON                           *
30    !* DATE:  16 NOVEMBER 1987                                               *
40    !* THESIS ADVISOR:  PROFESSOR A.A. ATCHLEY                               *
50    !* PROGRAM NAME:  CAVDAT                                                 *
60    !* PROGRAMMING LANGUAGE:  HP BASIC 5.0                                   *
70    !* COMPUTER:  HP 9000 SERIES 300                                         *
80    !*************************************************************************
90    !
100   !*******************************PURPOSE*********************************
110   !
120   !  THE PURPOSE OF "CAVDAT" IS TO CREATE AN ULTRASONIC SOUND FIELD
130   !  BY PROGRAMMING THE HP 3314A FUNCTION GENERATOR.  USER-DEFINED
140   !  PULSE BURSTS ARE SENT TO A FOCUSSED TRANSDUCER WHICH IS THEN
150   !  SWEPT THROUGH A USER-DEFINED AMPLITUDE RANGE.  THE USERS CAN THEN
160   !  DEVOTE THEIR ATTENTION TO DETECTION OF CAVITATION EVENTS DISPLAYED
170   !  ON AN OSCILLOSCOPE.  FURTHER, WHEN A CAVITATION EVENT IS DETECTED,
180   !  AND THE COMPUTER IS MANUALLY CUED, THE COMPUTER WILL DETERMINE
190   !  TRANSDUCER SOURCE LEVEL USING CONVERSION FACTORS PRE-DETERMINED
200   !  EXPERIMENTALLY.  THE CRITICAL USER INPUTS ARE PULSE REPETITION
210   !  FREQUENCY (PRF) AND PULSE DURATION.  THIS ALGORITHM WILL CALCULATE
220   !  THE REQUIRED NUMBER OF CYCLES PER BURST, N, TO ACHIEVE THE DESIRED
230   !  WAVEFORM SUBJECT TO THESE PARAMETERS.
240   !
250   !*************************VARIABLE DEFINITIONS*************************
260   !
270   !  Ampout = HP 3314A OUTPUT VOLTAGE AMPLITUDE IN MILLIVOLTS.
280   !  Ampstart = HP 3314A STARTING VOLTAGE AMPLITUDE IN MILLIVOLTS.
290   !  Gain = POWER AMPLIFIER GAIN.
300   !  Incr = HP 3314A VOLTAGE INCREMENT IN MILLIVOLTS.
310   !  Intvl = SW/TR INTERVAL IN MILLISECONDS.
320   !  N = NUMBER OF CYCLES IN PULSE BURST; HP 3314A IS IN N-CYCLE MODE.
330   !  K = COUNTER INDEX.
340   !  L = COUNTER INDEX.
350   !  Numbsteps = NUMBER OF STEPS IN VOLTAGE AMPLITUDE SWEEP.
360   !  Opfreq = TRANSDUCER OPERATING FREQUENCY.
370   !  Peak(K) = PEAK PRESSURE AT CAVITATION EVENT IN BAR.
380   !  Prf = PULSE REPETITION FREQUENCY IN HZ.
390   !  Pulse = PULSE DURATION IN MICROSECONDS.
400   !  Rem = REMAINDER OF THE INDICATED DIVISION.
410   !
420   CLEAR SCREEN
430   CLEAR 7  !CLEAR HP-IB INTERFACE
440   ON KBD ALL GOTO 1470  !ALLOW FOR USER INTERRUPT OF PROGRAM.
450   !
460   !*************************VARIABLE DECLARATIONS************************
470   !
480   INTEGER K,L,N,Numbsteps
490   REAL Ampout,Ampstart,Gain,Incr,Intvl,Opfreq,Prf,Pulse,Rem
500   !
```

```
510   !**********************DIMENSION LINEAR ARRAYS**********************
520   !
530   DIM Amplnc(1000),Peak(1000)
540   !
550   !*****************************ADDRESSES*****************************
560   !
570   !  717 IS THE ADDRESS OF THE HP 3314A FUNCTION GENERATOR.
580   !  702 IS THE ADDRESS OF THE HP 2225A THINKJET PRINTER.
590   !
600   !
610   !****************************IMPORTANT*****************************
620   !
630   !  PRIOR TO ANY TEST RUN, VERIFY POWER AMPLIFIER GAIN.
640   !
650   !*********************INPUT PULSE PARAMETERS*********************
660   !
670   CLEAR SCREEN
680   DISP "PLEASE ENTER TRANSDUCER OPERATING FREQUENCY IN KHZ.";
690   INPUT Opfreq
700   DISP "PLEASE ENTER POWER AMPLIFIER GAIN (200 OR LESS).";
710   INPUT Gain  !OPERATOR INPUTS THE GAIN FOR FUTURE REFERENCE.
720   IF Gain<200 THEN GOTO 740
730   GOTO 770
740   DISP "THIS GAIN MAY RESULT IN TRANSDUCER DAMAGE."
750   WAIT 2
760   GOTO 700
770   DISP "PLEASE ENTER DESIRED PULSE REPETITION FREQUENCY (IN HZ).";
780   INPUT Prf
790   Intvl=(1/Prf)*1000  !CALCULATE SW/TR INTERVAL IN MILLISECONDS.
800   DISP "PLEASE ENTER DESIRED PULSE DURATION IN MICROSECONDS.";
810   INPUT Pulse
820   N=((Pulse*Opfreq)/1000)  !CALCULATE NUMBER OF CYCLES.
830   !ECHO THE INPUT PARAMETERS AND ALLOW USER TO EDIT AS NECESSARY.
840   PRINT "TRANSDUCER OPERATING FREQUENCY IS:";Opfreq;"KHZ."
850   PRINT "PULSE REPETITION FREQUENCY IS:";Prf;"HZ."
860   PRINT "PULSE DURATION IS:";Pulse;"MICROSECONDS."
870   PRINT "NUMBER OF CYCLES PER BURST IS:";N
880   PRINT "POWER AMPLIFIER GAIN IS:";Gain
890   PRINT "SW/TR INTERVAL IS:";Intvl;"MILLISECONDS."
900   PRINT "ARE THESE PARAMETERS CORRECT? (Y/N)"
910   INPUT Dec1$
920   IF UPC$(Dec1$)="N" THEN GOTO 670
930   !
940   !*********************INPUT SWEEP PARAMETERS*********************
950   !
960   CLEAR SCREEN
970   DISP "PLEASE INPUT SWEEP STARTING AMPLITUDE IN MILLIVOLTS.";
980   INPUT Ampstart
990   DISP "PLEASE INPUT AMPLITUDE INCREMENT IN MILLIVOLTS.";
1000  INPUT Incr
```

```
1010  DISP "PLEASE INPUT NUMBER OF STEPS PER SWEEP";
1020  INPUT Numbsteps
1030  IF Ampstart<3000 THEN GOTO 1070
1040  IF Numbsteps*Incr>3000 THEN GOTO 1070
1050  IF Ampstart+(Numbsteps*Incr)>3000 THEN GOTO 1070
1060  GOTO 1130
1070  DISP "ENTRY OF THESE PARAMETERS MAY RESULT IN TRANSDUCER DAMAGE."
1080  WAIT 2
1090  GOTO 960
1100  !
1110  !ECHO THE SWEEP PARAMETERS.
1120  !
1130  PRINT "STARTING AMPLITUDE IS:";Ampstart;"MILLIVOLTS."
1140  PRINT "AMPLITUDE INCREMENT IS:";Incr;"MILLIVOLTS."
1150  PRINT "NUMBER OF STEPS PER SWEEP IS:";Numbsteps
1160  PRINT "ARE THESE PARAMETERS CORRECT? (Y/N).";
1170  INPUT Dec2$
1180  IF UPC$(Dec2$)="N" THEN GOTO 960
1190  k=1  !INITIALIZE STORAGE FIELD COUNTER.
1200  !
1210  !*********************AMPLITUDE SWEEP INFORMATION*********************
1220  !
1230  CLEAR SCREEN
1240  OUTPUT 717;"FR";Opfreq;"KZ"  !SET TRANSDUCER OPERATING FREQUENCY.
1250  OUTPUT 717;"MO3"  !SET N-CYCLE MODE.
1260  OUTPUT 717;"NM";N;"EN"  !SET NUMBER OF CYCLES.
1270  OUTPUT 717;"TI";Intvl;"MS"  !SET SW/TR INTERVAL.
1280  WAIT 1  !ALLOW TRANSIENTS TO SETTLE OUT.
1290  Ampout=Ampstart
1300  FOR I=1 TO Numbsteps STEP 1  !COMMENCE AMPLITUDE SWEEP.
1310  Ampinc(I)=Ampout
1320  OUTPUT 717;"AP";Ampinc(I);"MV0"  !SET FUNCTION GENERATOR.
1330  Ampout=Ampinc(I)+Incr  !INCREMENT COUNTER.
1340  WAIT 1.5  !ALLOW TRANSIENTS TO SETTLE OUT.
1350  NEXT I  !CONTINUE WITH SWEEP UNTIL COMPLETE.
1360  PRINT "AMPLITUDE SWEEP COMPLETE."
1370  IF Opfreq=986 THEN GOTO 1390
1380  IF Opfreq=2170 THEN GOTO 1410
1390  Peak(K)=(.0522*((Ampout-Incr)*(.2)))
1400  GOTO 1420
1410  Peak(K)=(.0403*((Ampout-Incr)*(.2)))
1420  PRINT "SINCE NO EVENT DETECTED, THRESHOLD IS GREATER THAN:";Peak(K);"BAR.
1430  GOTO 1580  !QUERY USER FOR FURTHER INSTRUCTIONS.
1440  !
1450  !*********************CAVITATION INFORMATION*********************
1460  !
1470  DISP "WAS A CAVITATION EVENT DETECTED?";
1480  INPUT Dec3$
1490  IF UPC$(Dec3$)="N" THEN GOTO 1580
1500  IF UPC$(Dec3$)="Y" THEN GOTO 1510
```

```
1510  IF Opfreq=985 THEN GOTO 1530
1520  IF Opfreq=2170 THEN GOTO 1550
1530  Peak(K)=(.0522*(Ampinc(I)*(.2)))
1540  GOTO 1560
1550  Peak(K)=(.0403*(Ampinc(I)*.2)))
1560  PRINT "PEAK PRESSURE AT CAVITATION EVENT NUMBER";K;"IS:";Peak(K);"BAR."
1570  K=K+1
1580  DISP "DO YOU WISH TO RUN AGAIN WITH THE SAME PARAMETERS?";
1590  INPUT Dec4$
1600  IF UPC$(Dec4$)="Y" THEN GOTO 1620
1610  IF UPC$(Dec4$)="N" THEN GOTO 1740
1620  OUTPUT 717;"PR"  !RESET HP 3314A FUNCTION GENERATOR.
1630  WAIT 50  !ESTABLISH QUIESCENT PERIOD BETWEEN TRIALS.
1640  BEEP 976.56,1   !CUE USER THAT ANOTHER TRIAL IS ABOUT TO START.
1650  BEEP 1302.08,.5
1660  BEEP 1546.22,.5
1670  BEEP 1790.35,.75
1680  BEEP 1302.08,.25
1690  BEEP 1790.36,1
1700  GOTO 1240
1710  !
1720  !*************************PRINT-OUT OPTION*************************
1730  !
1740  DISP "WOULD YOU LIKE A HARD COPY OF PARAMETERS AND RESULTS?";
1750  INPUT Dec5$
1760  IF UPC$(Dec5$)="Y" THEN GOTO 1780
1770  IF UPC$(Dec5$)="N" THEN GOTO 1920
1780  PRINTER IS 702  !IDENTIFY ADDRESS OF THINKJET PRINTER.
1790  PRINT "TRANSDUCER OPERATING FREQUENCY IS:";Opfreq;"KHZ."
1800  PRINT "NUMBER OF CYCLES PER BURST IS:";N
1810  PRINT "POWER AMPLIFIER GAIN IS:";Gain
1820  PRINT "SW/TR INTERVAL IS:";Intvl;"MILLISECONDS."
1830  PRINT "PULSE DURATION IS:";Pulse;"MICROSECONDS."
1840  PRINT "PULSE REPETITION FREQUENCY IS:";Prf;"HZ."
1850  FOR L=1 TO (K-1) STEP 1  !CREATE DO LOOP FOR PRINTING OF RECORDED EVENTS.
1860  PRINT "PEAK PRESSURE AT CAVITATION EVENT NUMBER";L;"IS";Peak(L);"BAR."
1870  NEXT L  !CONTINUE UNTIL COMPLETE.
1880  PRINTER IS CRT  !RETURN TO CRT
1890  !
1900  !******************CONTINUE TESTING IF NECESSARY******************
1910  !
1920  DISP "DO YOU WISH TO ALTER PARAMETERS AND RUN AGAIN?";
1930  INPUT Dec6$
1940  IF UPC$(Dec6$)="Y" THEN GOTO 1960
1950  IF UPC$(Dec6$)="N" THEN GOTO 2050
1960  OUTPUT 717;"PR"  !RESET HP 3314A FUNCTION GENERATOR.
1970  WAIT 60  !ESTABLISH QUIESCENT PERIOD BETWEEN TRIALS.
1980  BEEP 976.56,1  !CUE USER THAT ANOTHER TRIAL IS ABOUT TO START.
1990  BEEP 1302.08,.5
2000  BEEP 1546.22,.5
```

```
2010  BEEP 1790.36,.75
2020  BEEP 1302.08,.25
2030  BEEP 1790.36,1
2040  GOTO 870
2050  PRINT "PROGRAM COMPLETE."
2060  OUTPUT 717;"PR"  !RESET HP 3314A FUNCTION GENERATOR.
2070  END
```

APPENDIX B

PVDF HYDROPHONE CONSTRUCTION AND GENERAL INFORMATION

A. CONSTRUCTION DETAILS

Our desire for small size led us to choose a large plastic syringe and a large–diameter hypodermic needle as the hydrophone housing. This gave us a convenient method for insulating the "hot" lead from the grounded elements, as well as providing ample storage area close to the active elements for the preamplifier circuitry. Our primary difficulty in construction was working with small sizes of PVDF film. After numerous unsuccessful attempts to cut the PVDF to a shape which allowed for good electrical connection while minimizing active element size (1 mm^2), we moved to a PVDF strip approximately 2 mm wide and about 4 cm in length. We reduced the bottom (positive) side of the film by etching away the PVDF using a Q-tip soaked in ferric chloride, which gave us a marginally accurate method of reducing element size while keeping a capability to have a reliable electrical connection. The top (ground) was not etched. The PVDF strip was then centered on a 3.6 mm x 6.4 mm brass plate attached to the "hot" lead. The barrel of the needle was insulated with several layers of heat shrink tubing to prevent any of the "hot" side from short–circuiting to ground. The remaining lengths of the PVDF strip were attached to the insulation along the needle barrel and connected to the surface of the needle with nickel paint. Gaps between the PVDF strip and needle

were filled with epoxy adhesive to add stability. Resistance measurements were taken to ensure continuity of connections and that no short circuits existed. The unity gain preamplifier (voltage follower) was constructed and installed in the syringe and electrical connections made to the hot lead and external ground connections. The entire apparatus was insulated by being coated with "Plasti-Dip." See Figures B.1 and B.2.

B. SENSITIVITY CALCULATION [Ref. 28]

$E = V_0/t$ where E = Electric Field developed

V_0 = Voltage Induced

t = Thickness of Piezoelectric film

Also, $E = g_{33}X_3$ where g_{33} is a constant indicating field/applied stress

X_3 = Applied mechanical stress

$$M_0 = \text{Pressure Sensitivity} = V/P = \frac{(Et)}{X_3} = \frac{g_{33}X_3t}{X_3} = g_{33}t$$

Numerically,

$$M_0 = g_{33}t = 339 \times 10^{-3} \frac{(V/m)}{(N/m^2)} \times (9 \times 10^{-6}\ m)$$

$$= 3.051 \times 10^{-6} \frac{V}{N/m^2} = 3.051 \times 10^{-6} \frac{V}{Pa}$$

$M_0 = 20 \log_{10} (3.051 \times 10^{-6})$ dB re 1V/Pa = −110.31 dB re 1V/Pa

Figure B.1

PVDF Hydrophone

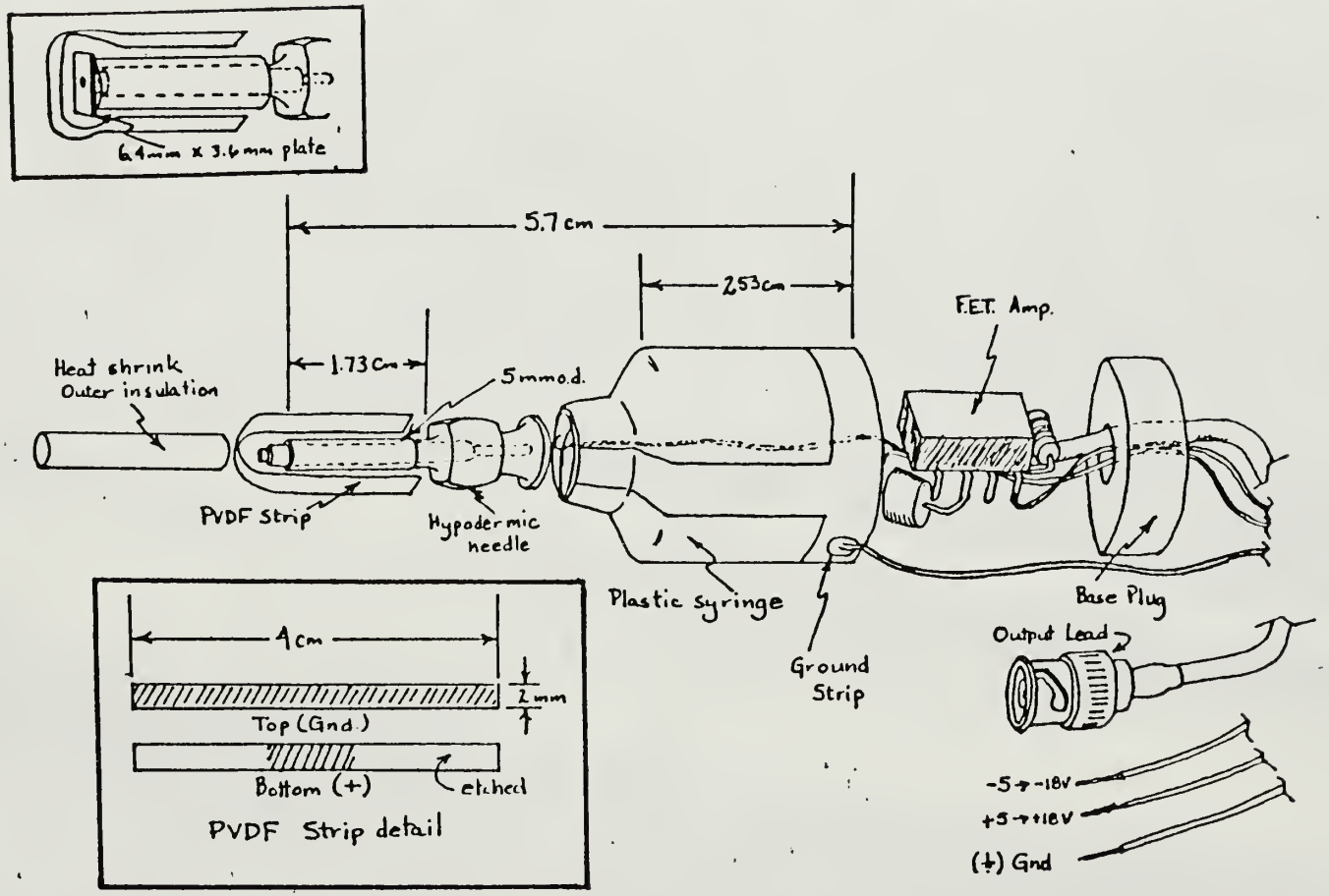

Figure B.2

Exploded Drawing of PVDF Hydrophone

This calculation indicates that transducer pressure sensitivity is frequency independent. It should be mentioned that the calculated sensitivity is contingent upon the assumption that the nickel paint used to mount the PVDF to the brass mounting block effectively clamps the active face in the (1) and (2) directions, thus confining the face to operation solely in the thickness–expander mode. See Figure B.3.

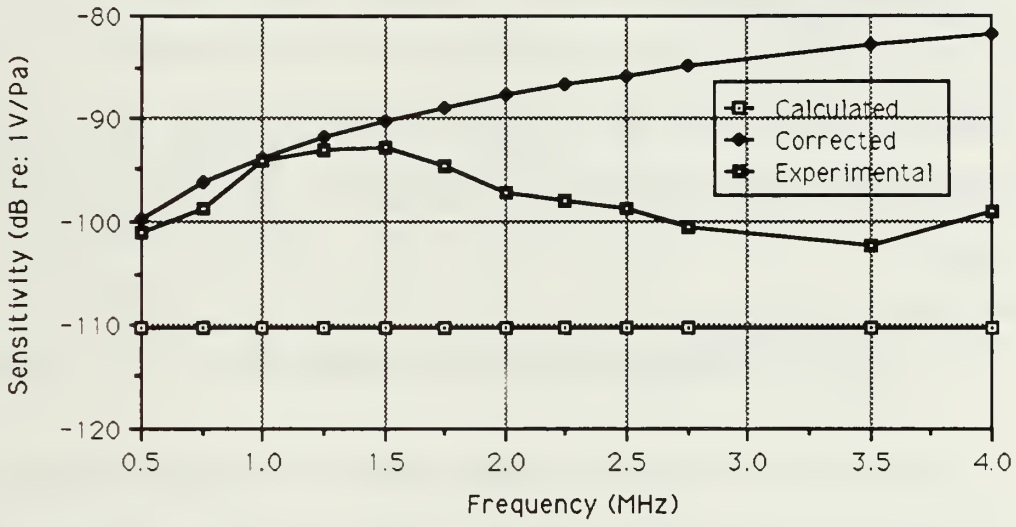

Figure B.3

PVDF Hydrophone Sensitivity Calibration Curves

C. DESCRIPTION OF TEST AND CALIBRATION TECHNIQUE

We chose the reciprocity technique for calibration of our hydrophone sensitivity because calibrated hydrophones in the megahertz range were not available for comparison. Our frequency band of interest was 0.5 MHz to 4.0 MHz. For the reciprocity calibration, we used two Panametric V323 transducers as the trans-

mitting and reversible elements of the experimental setup. These transducers are designed for operation at 2.25 MHz and provided smooth response through the frequency range. The calibration set up was as noted in the equipment diagram included as Figure 4.1. The distance between the transducers was 30 cm, which is well into the far field for all frequencies of interest. Far-field calculation for the maximum frequency is as follows:

$$r = \frac{L^2}{4\lambda} \text{ [Ref. 25]}$$

where $L = 5 \times 10^{-3}$, m = largest extent of source active element, λ = wavelength at 4.0 MHz in fresh water, r = minimum extent of far field, and

$$r = \frac{(5 \times 10^{-3}\text{m})^2}{4(3.70 \times 10^{-4}\text{m})} = 0.1689 \text{ m} = 16.89 \text{ cm}$$

We took Voltage Level (in dBV) and input current (in milli-amperes) readings from the HP 3585A Spectrum Analyzer and HP 3478A Digital Multimeter in accordance with standard reciprocity techniques.

Open-circuit voltage sensitivity of our PVDF hydrophone was determined using the following equation:

$$M_{0X} = \left(\left(\frac{2\lambda r}{\rho_0 c} \right) \left(\frac{V_X V_X'}{V_R I_R} \right) \right)^{1/2} \text{ [Ref. 25]}$$

When converted to sensitivity level, this calculation became:

$$ML = \left[V_{L_R} + V_{L_X}' - V_{L_R} - I_{L_R} - 20 \log f + 20 \log \frac{2r}{\rho 0} \right] x \frac{1}{2}$$

D. DIRECTIVITY EFFECTS/EXCITATION OF FIRST THICKNESS MODE

1. Analysis of Directivity Effects

One possible cause of the difference between actual and predicted sensitivities may be the change in the directivity of the hydrophone as frequency increases. As the transmitting transducer frequency is increased, both the hydrophone and transducer become more directional, implying more efficient transmission by the transducer and more efficient reception by the hydrophone of the acoustic power in a given direction. The trade-off is that the main lobes of both the transducer and the hydrophone become narrower. Using the approximation for a piston-like source [Ref. 25],

$D \approx 1/4\ k^2 L_1 L_2$ where $L_1 \cong 2$ mm and $L_2 \cong 5$ mm

$k = \omega/c = 2\pi f/c$

At 500 kHz, $DI = 10 \log D = 10.5$ dB

These "corrected" calculated values are plotted as such in Figure B.3.

2. Calculation of First Thickness Mode of Brass Mounting Plate

It was originally believed that the brass mounting plate would behave as if it were perfectly rigid in the frequency range of interest. Measurements led us to believe that this may not be the case. For this

reason, it was decided to determine if the first thickness mode of the brass mounting plate was being excited somewhere in the range between 0.5 MHz and 4.0 MHz. The first thickness mode will be excited with $t = \lambda/2$ or when $\lambda = 2t$. For a thickness of 1.3 mm, λ = 2.6 mm. Since $c = f\lambda$, $f = c/\lambda$:

$$f = c/\lambda = (4700 \text{ m/s})/2.6 \times 10^{-3} \text{ m} \cong 1.81 \text{ MHz}$$

It becomes evident that it is likely that the first thickness mode is being excited to some extent.

E. DISCUSSION

As noted above, theoretical sensitivity was calculated assuming that the longitudinal and transverse modes were clamped and that only the thickness mode was excited. Data showed little agreement with these original theoretical calculations, however. The PVDF hydrophone's active face was considerably larger than the wavelengths of the frequencies of interest, which makes the receiving beam pattern more narrow as the frequency increases. This directivity also adds considerably to the sensitivity when sound is received "on axis." Directivity and Directivity Index as calculated previously in this paper contributed greatly to the sensitivity of the hydrophone. As can be seen from the graph of Pressure Sensitivity vs. Frequency (See Figure B.3), there is good agreement between theoretical and experimental values at the lower end of the frequency range (up to 1.5 MHz). At higher frequencies, additional variables are introduced which limit

agreement. A likely contributor to the higher frequency disparity might be slight misalignment of the hydrophone. As frequency goes up, the beam pattern becomes increasingly narrow. Slight misalignment could result in poorer reception of the transmitted acoustic energy. Lastly, as alluded to previously, it is possible that the first thickness mode of the brass mounting plate is being excited in the frequency range of interest.

LIST OF REFERENCES

1. Ross, D., Mechanics of Underwater Noise, p. 202, Pergamon Press, Inc., 1976.

2. Strasberg, M., "Onset of Ultrasonic Cavitation Tap Water," Journal of the Acoustical Society of America, v. 31, pp. 163-176, February 1959.

3. Apfel, R. E., "Possibility of Microcavitation from Diagnostic Ultrasound," IEEE Transactions on Ultrasonics, Ferroelectrics, and Frequency Control, v. UFFC-33, pp. 140-146, March 1986.

4. Flynn, H. G., "Generation of Transient Cavities in Liquids by Microsecond Pulses of Ultrasound," Journal of the Acoustical Society of America, v. 72, pp. 1926-1932, December 1982.

5. Roy, R. A., Atchley, A. A., Crum, L. A., Fowlkes, J. B., and Reidy, J. J., "A Precise Technique for the Measurement of Acoustic Cavitation Thresholds and Some Preliminary Results," Journal of the Acoustical Society of America, v. 78, pp. 1799-1805, November 1985.

6. Atchley, A. A., Frizzell, L. A., and Apfel, R. E., "Thresholds for Cavitation Produced in Water by Pulsed Ultrasound," submitted for publication in Ultrasonics.

7. Walton, A. J., and Reynolds, G. T., "Sonoluminescence," Advances in Physics, v. 33, pp. 595-660, 1984.

8. Neppiras, E. A., and Noltingk, B. E., "The Onset of Cavitation Produced by Ultrasonics," Proceedings of the Physical Society of London Section B, v. 64, pp. 1032-1038, 1951.

9. Harvard University Acoustics Research Laboratory Technical Memorandum No. 12, The Onset of Cavitation in Liquids: I, by F. G. Blake, Jr., p. 28, 2 September 1949.

10. Rayleigh, Lord, "On the Pressure Developed in a Liquid During the Collapse of a Spherical Cavity," Philosophy Magazine, v. 34, pp. 94-98, August 1917.

11. Plesset, M. S., "The Dynamics of Cavitation Bubbles," Journal of Applied Mechanics, v. 16, pp. 277-282, September 1949.

12. Poritsky, H., "The Collapse or Growth of a Spherical Bubble or Cavity in a Viscous Fluid," Proceedings of the First U.S. National Congress on Applied Mechanics, ed. E. Sternberg (New York), pp. 813-821, 1952.

13. Noltingk, B. E., and Neppiras, E. A., "Cavitation Produced by Ultrasonics," Proceedings of the Physical Society of London Section B, v. 63, pp. 674-685, 1950.

14. Lauterborn, W., "Numerical Investigation of Nonlinear Oscillations of Gas Bubbles in Liquids," Journal of the Acoustical Society of America, v. 59, pp. 283-293, February 1976.

15. Crum, L. A., "Rectified Diffusion," Ultrasonics, v. 22, pp. 215-223, September 1984.

16. Harvey, E. N., Barnes, D. K., McElroy, W. D., Whitely, A. H., Pease, D. C., and Cooper, K. W., "Bubble Formation in Animals," Journal of Cellular and Comparative Physiology, v. 24, pp. 1-40, 1944.

17. Griffing, V., "Theoretical Explanation of the Chemical Effects of Ultrasonics," Journal of Chemical Physics, v. 18, pp. 997-998, 1950.

18. Sehgal, C., Steer, R. P., Sutherland, R. G., and Verrall, R. E., "Sonoluminescence of Aqueous Solutions," Journal of Physical Chemistry, v. 81, pp. 2618-2620, December 1977.

19. Sehgal, C., Sutherland, R. G., and Verrall, R. E., "Optical Spectra of Sonoluminescence from Transient and Stable Cavitation in Water Saturated with Various Gases," Journal of Physical Chemistry, v. 84, pp. 388-395, February 1980.

20. Sehgal, C., and Verrall, R. E., "A Review of the Electrical Hypothesis of Sonoluminescence," Ultrasonics, v. 20, pp. 37-39, January 1982.

21. Vaughan, P., and Leeman, S., "Some Comments on Mechanisms of Sonoluminescence," Acustica, v. 59, pp. 279-281, 1986.

22. Crum, L. A., and Reynolds, G. T., "Sonoluminescence Produced by Stable Cavitation," Journal of the Acoustical Society of America, v. 78, pp. 137-139, July 1985.

23. Daniels, F., and Alberty, R. A., Physical Chemistry, 4th ed., p. 328, John Wiley & Sons, Inc., 1975.

24. Clay, C. S., and Medwin, H., Acoustical Oceanography: Principles and Applications, pp. 184-204, John Wiley & Sons, Inc., 1977.

25. Kinsler, L. E., and others, Fundamentals of Acoustics, 3rd ed., pp. 389-391, John Wiley & Sons, Inc., 1982.

26. Dunn, F., Averbuch, A. J., and O'Brien, W. D., "A Primary Method for the Determination of Ultrasonic Intensity With the Elastic Sphere Radiometer," Acustica, v. 38, pp. 58-61, 1977.

27. Lindsay, R. B., Mechanical Radiation, pp. 217, 292-293, McGraw-Hill Book Co., 1960.

28. Pennwalt Corporation, KYNAR™ Piezo Film Technical Manual, 1983.

INITIAL DISTRIBUTION LIST

		No. Copies
1.	Defense Technical Information Center Cameron Station Alexandria, VA 22304-6145	2
2.	Library Code 0142 Naval Postgraduate School Monterey, CA 93943-5000	2
3.	Dr. L. E. Hargrove Office of Naval Research Physics Division - Code 1112 800 N. Quincy Street Arlington, VA 22217	1
4.	Commander, Naval Coastal Systems Center Dr. Elan Moritz - Code 4120 Panama City, FL 32407-5000	1
5.	Professor A. A. Atchley, Code 61Ay Naval Postgraduate School Monterey, CA 93943-5000	4
6.	Professor S. R. Baker, Code 61Ba Naval Postgraduate School Monterey, CA 93943-5000	1
7.	Professor S. L. Garrett, Code 61Gx Naval Postgraduate School Monterey, CA 93943-5000	1
8.	Chairman, Department of Physics, Code 61 Naval Postgraduate School Monterey, CA 93943-5000	1
9.	LCDR R. L. Bruce 6002 Crocus Court Alexandria, VA 22310	3
10.	LT R. D. Middleton, Jr. 141 John Street Hauppauge, NY 11787	5

11. Amy and Aaron Bruce 1
213 Brookdale Drive
League City, TX 77573

12. CAPT Robert Perron 1
Department of Physics
Naval Postgraduate School
Monterey, CA 93943-5000

13. Mr. and Mrs. R. D. Middleton, Sr. 1
141 John Street
Hauppauge, NY 11787

14. Maris R. Zanger 1
300 Glenwood Circle #164
Monterey, CA 93940

Thesis
B82475 Bruce
c.1 An investigation of acoustic cavitation produced by pulsed ultrasound.